Six years of UARS Microwave Limb Sounder HNO_3 observations: Seasonal, interhemispheric, and interannual variations in the lower stratosphere

M. L. Santee, G. L. Manney, L. Froidevaux, W. G. Read, and J. W. Waters
Jet Propulsion Laboratory, California Institute of Technology, Pasadena.

Short title: MICROWAVE LIMB SOUNDER HNO_3 VARIATIONS

Abstract. We present an overview of the seasonal, interhemispheric, and interannual variations in the distribution of HNO_3 in the lower stratosphere based on measurements of gas-phase HNO_3 made by the UARS Microwave Limb Sounder (MLS) through six complete annual cycles in both hemispheres. Outside of the winter polar regions, zonal-mean HNO_3 mixing ratios on the 465-K potential temperature surface are comparable in the two hemispheres in all latitude bands and in all years examined. Except at high latitudes, interannual variability is minimal, and there is no significant hemispheric asymmetry in the overall HNO_3 distribution or its seasonal cycle. Although the Antarctic experiences widespread severe denitrification, the MLS data indicate that the denitrification is not complete; that is, not all polar stratospheric cloud (PSC) particles sediment out of the lower stratosphere. Renitrification at 465 K during the mid- to late-winter period (when temperatures, though still low, are generally rising) is most likely achieved through a combination of PSC evaporation and continuing weak diabatic descent. Despite large interhemispheric and interannual differences in the extent and duration of PSC activity and denitrification, HNO_3 recovers to similar values at the end of every winter in both the Arctic and the Antarctic. Zonal-mean HNO_3 values for the two hemispheres are virtually indistinguishable for the latitudes equatorward of 65°, even during the winter months. Thus the effects of severe denitrification are confined in both space and time to the regions poleward of 65°S during the winter and early spring.

1. Introduction

The principal cause of the ozone loss that occurs in the polar lower stratosphere during late winter and early spring is known to be chlorine chemistry [e.g., *Solomon*, 1990]. Although ozone depletion over the Arctic has been significant in recent years [e.g., *Manney et al.*, 1996a; *Donovan et al.*, 1996; *Müller et al.*, 1996], it has never been as severe as that over Antarctica, despite the fact that abundances of reactive chlorine comparable to those over Antarctica have been observed throughout the Arctic vortex [*Waters et al.*, 1993]. Nitric acid (HNO_3) plays a pivotal role in determining the cumulative amount of ozone loss [e.g., *Solomon*, 1990]. It is a key component of the polar stratospheric clouds (PSCs) that form in the low temperatures of polar winter, removing HNO_3 from the gas phase. PSC particles provide surfaces on which heterogeneous reactions occur, facilitating the conversion of chlorine from its reservoir species (e.g., $ClONO_2$, HCl) to the highly reactive forms that participate in the catalytic cycles of ozone destruction (e.g., ClO). On the other hand, photolysis of HNO_3 vapor releases NO_2, enabling a major pathway for the deactivation of chlorine, via the reformation of $ClONO_2$ from ClO and NO_2. Thus, as a central participant in both the activation and the deactivation of chlorine, HNO_3 indirectly regulates the extent and duration of ozone depletion.

The abundance of available reactive nitrogen is reduced both through the direct incorporation of HNO_3 into PSC particles and through the heterogeneous conversion of other nitrogen-containing species into HNO_3 that is then bound in the PSCs [e.g., *Turco et al.*, 1989]. The HNO_3 may be only temporarily sequestered and then released back to the gas phase as temperatures rise and the clouds evaporate. But if the PSC particles grow sufficiently large, appreciable sedimentation can occur, leading to denitrification, the permanent removal of reactive nitrogen from the lower stratosphere. A substantial reduction in the amount of available reactive nitrogen facilitates persistence of high ClO levels and thus allows the chlorine-catalyzed destruction of ozone to continue.

Significant dissimilarities in seasonal temperature patterns and vortex behavior exist between the northern and southern hemispheres [e.g., *Andrews*, 1989; *Waugh and Randel*,

1998]. On average, lower stratospheric temperatures are ~15–20 K higher, and the vortex is weaker and more distorted, in the Arctic than in the Antarctic, leading to fewer and less persistent PSC events in the Arctic [*Poole and Pitts*, 1994]. The different meteorological conditions in the two hemispheres give rise to very dissimilar patterns of denitrification. In situ [e.g., *Fahey et al.*, 1990] and satellite [*Roche et al.*, 1994; *Santee et al.*, 1995] observations have revealed that both the temporal and the spatial scale of denitrification are substantially greater in the Antarctic than in the Arctic. These differences in the morphology of HNO_3 have profound implications, since the interhemispheric differences in the severity of ozone loss can be largely ascribed to the moderating influence of high levels of HNO_3 throughout the Arctic winter [e.g., *Brune et al.*, 1991; *Santee et al.*, 1995].

Much has been learned about the behavior of HNO_3 since it was first detected in the stratosphere 30 years ago [*Murcray et al.*, 1968]. For instance, a wealth of information about its latitudinal gradients and seasonal variations, in particular its buildup and depletion in the winter polar regions, has been obtained from studies of ground-based, aircraft, and satellite data. However, none of these data sets have allowed the full hemispheric evolution of HNO_3 over complete annual cycles to be studied. Several questions about the general behavior of HNO_3 remain unanswered. One issue of relevance to stratospheric ozone depletion, particularly in the Antarctic, is whether there is closure in the HNO_3 abundances over an annual cycle; that is, have HNO_3 values at the end of the springtime recovery period rebounded to unperturbed levels or is the stratosphere experiencing a gradual decline in reactive nitrogen, if HNO_3 lost through PSC sedimentation is not replaced? What is the degree of interannual variability in the HNO_3 buildup, depletion, and recovery at high latitudes? Is the denitrification in the Antarctic vortex complete; that is, do all of the PSC particles that form eventually settle out? Does the severe denitrification in the Antarctic vortex have a strong influence on midlatitudes, either during or after the winter season? Is there a significant hemispheric asymmetry in the overall HNO_3 distribution or its seasonal cycle?

With the long-term data record from the Upper Atmosphere Research Satellite (UARS),

we now have the opportunity to address these questions. Two instruments on UARS provided global measurements of gas-phase HNO_3 in the lower stratosphere: the Cryogenic Limb Array Etalon Spectrometer (CLAES) and the Microwave Limb Sounder (MLS). CLAES made HNO_3 measurements through two northern and one southern winter [*Roche et al.*, 1994] before its stored supply of cryogen was depleted. We present here the MLS HNO_3 measurements. MLS has made HNO_3 measurements through more than six complete annual cycles in both hemispheres, although its temporal sampling has become sparser in recent years. This MLS HNO_3 data set, unprecedented in its scope, is uniquely suited to studying the seasonal, interhemispheric, and interannual variations in the distribution of HNO_3 in the lower stratosphere.

2. Measurement Description

2.1. MLS Data Coverage

MLS has been acquiring millimeter-wavelength emission measurements of the stratosphere in both hemispheres since late September 1991. The microwave limb sounding technique and the MLS instrument are described in detail by *Waters* [1993] and *Barath et al.* [1993], respectively. Advantages of this technique include the measurement of thermal emission, so that observations can be obtained both day and night, and the use of long wavelengths, so that the data are not degraded by the presence of PSCs or other stratospheric aerosols (see, e.g., Figure 3 of *Waters et al.* [1998]). The latter point is particularly important since HNO_3 is a major component of PSCs and since the time period examined here encompasses the dissipation phase of the aerosol associated with the eruption of Mount Pinatubo.

The MLS pointing geometry together with the inclination of the UARS orbit leads to a measurement latitudinal coverage extending from 80° on one side of the equator to 34° on the other. The UARS orbit plane precesses in such a way that all local solar times are sampled in

~36 days (a "UARS month"), getting ~20 min earlier each day at a given latitude. To keep MLS (and other instruments) on the shaded side of the spacecraft, a 180° yaw maneuver is performed at the end of every UARS month. Thus 10 times per year MLS alternates between viewing northern and southern high latitudes, with the first day of a particular UARS month occurring ~5 days earlier each year. As a consequence, on a particular day of the year MLS may have been viewing northern high latitudes in some years but southern high latitudes in other years.

At the time of writing, MLS has observed six southern hemisphere and seven northern hemisphere winters. However, problems with the UARS solar array caused the MLS instrument to be turned off during much of the early southern winter observing period in 1992. By early 1994, the MLS antenna scanning mechanism began to exhibit signs of wear, and March, April, May, and July 1994 were primarily devoted to testing new operational modes, with significantly reduced data sampling. Similarly, a combination of continuing difficulties with the MLS scan system and problems with the spacecraft batteries and solar array led to severely limited data-gathering from October 1994 through July 1995. Various modifications to the operation of the antenna scanning mechanism were implemented in February 1995, and in June of that year an MLS operational schedule consisting of (typically) two days of scanning followed by one day of "rest" was adopted to conserve lifetime. In May 1995, the solar array was parked because of problems with both the primary and the redundant drive systems. This resulted in a reduction in available power, and UARS began operating in an instrument power sharing mode whereby MLS is periodically turned off. In May 1997 the UARS onboard computer experienced an autonomous shutdown, stressing the batteries and prompting one (of three) to be removed from service. Because of the continuing degradation in the UARS power situation, MLS measurements were collected on only six days total during the months of May and June. After June 1997, the 63-GHz radiometer used to provide tangent pressure and temperature information during nominal operations was turned off to save power. Although HNO_3 and other standard products are still retrieved, offsets between these data and

those from the previous years are presently under investigation, and no data obtained after June 1997 are discussed here.

2.2. MLS HNO_3 Data Quality

The measurement of HNO_3 was not a primary MLS objective. However, a significant HNO_3 feature situated just outside the spectral region used to measure ozone imposes a weak slope through the 205-GHz ozone band that can be used to retrieve profiles of gas-phase HNO_3 over a limited vertical range in the lower stratosphere. MLS HNO_3 measurements from precursory retrieval algorithms were first presented by *Santee et al.* [1995]; version 4 MLS HNO_3 data for the 1995–1996 and 1996–1997 Arctic winters have been presented by *Santee et al.* [1996b] and *Santee et al.* [1997], respectively. In addition, *Santee et al.* [1998] present version 4 HNO_3 data from the 1992–1996 Antarctic winters; more extensive information about the HNO_3 retrievals and their quality and resolution is also included in that paper. Further details about the quality of the MLS data can also be obtained from the NASA Goddard Space Flight Center Distributed Access Archive Center (DAAC) as well as the MLS web page (http://mls.jpl.nasa.gov).

Preliminary validation studies indicate that the version 4 MLS HNO_3 data are scientifically useful on the 100-, 46-, and 22-hPa retrieval surfaces, where the estimated precisions for an individual profile are approximately 2.0, 3.0, and 4.5 ppbv, respectively. The precisions, estimated from several months of data, were based on the observed variability in a narrow latitude band centered around the equator that was selected to minimize the effects of natural atmospheric variability. The true precisions may be slightly better than these estimates since the actual atmospheric variation is not completely negligible. These empirical precisions are generally consistent with uncertainties derived theoretically by propagating the measurement noise through the retrieval algorithm. Although the computed uncertainties consist of both random and systematic components, the random (noise) components usually dominate for HNO_3, which has a relatively weak signal (compared with ozone, for example).

Since in this paper we will be most concerned with relative variations, the systematic errors are of less importance. The noise contribution to the uncertainty can be reduced by averaging together individual measurements. Most of the results shown in this study have been derived through averaging many individual data points, both zonally and temporally, and are therefore characterized by much better precision values (~0.5 ppbv or less) than those given above.

Initial comparisons (over a limited data set) with colocated UARS CLAES observations [*Kumer et al.*, 1996] show that there is good correspondence in the morphology of the CLAES and MLS HNO_3 fields. However, the version 4 MLS data appear to overestimate winter polar HNO_3 abundances (in the non-denitrified areas) by several ppbv; this behavior is seen at all three retrieval pressure levels but is particularly pronounced at 22 hPa, where the difference between the MLS and CLAES fields can exceed 5 ppbv. Preliminary comparisons with other correlative data sets also indicate that MLS overestimates HNO_3 abundances near the profile peak (~25 km). Development and validation of improved data processing algorithms for MLS HNO_3 are in progress.

3. Morphology and Synoptic Behavior

3.1. Daily Maps

As discussed in section 2.1, in any given year UARS performs 10 yaw maneuvers, so that MLS spends 5 UARS months viewing northern high latitudes and 5 viewing southern high latitudes. To examine the seasonal changes in HNO_3 and their repeatability from year to year, we have selected representative days from each yaw period. In an effort to maximize comparability, we have tried to choose days for which MLS data exist in all years under consideration. However, this process is complicated by the 5-day drift in the start of the UARS months from one year to the next, the data gaps arising from problems with the UARS solar array and the MLS antenna scanning mechanism, and the continuing deterioration in the UARS power situation, which has led to ever-sparser temporal coverage in the last few years.

In general, it was necessary to vary the dates slightly from year to year, with the largest range between dates in different years being 4 days, but for some yaw periods missing years were unavoidable. Each yaw period has at least 4 and at most 6 years represented. The selected days for the southern hemisphere are compiled in Table 1 and their corresponding maps are shown in Plate 1. The maps for each year are arranged to begin with early-April, at the beginning of the southern winter season, and end with mid-January, in southern summer. Similarly, the selected days for the northern hemisphere are compiled in Table 2 and shown in Plate 2, starting in northern fall and ending in northern summer for each year.

The MLS data in Plates 1 and 2 were gridded by binning and averaging 24 hours of data. The data were then interpolated onto the 465-K potential temperature (θ) surface (using United Kingdom Meteorological Office (UKMO) temperatures [*Swinbank and O'Neill*, 1994]) to reduce the effects of adiabatic vertical motions on the comparisons of data from different seasons and different years. The 465-K θ surface corresponds to a pressure range of ~30 to 60 hPa for the low temperatures inside the winter polar vortex and ~60 to 90 hPa for typical summertime temperatures. We primarily focus on the behavior of HNO_3 at these levels because of the apparently significant high bias in the MLS data at higher altitudes (see section 2.2). Superimposed on the maps are (in white) two contours of potential vorticity (PV) derived from the UKMO analyses to illustrate the size, shape, and strength of the polar vortex and (in black) two contours of UKMO temperature to represent the approximate thresholds for the formation of type I (195 K) and type II (188 K) PSCs.

Much can be observed about the distribution of HNO_3 in the lower stratosphere from inspection of Plates 1 and 2. Most generally, HNO_3 abundances increase from the equator to the pole (with the exception of the PSC-formation regions, discussed further below) in both hemispheres and in all seasons. This latitudinal variation in HNO_3 has been noted previously in aircraft [e.g., *Lazrus and Gandrud*, 1974; *Murcray et al.*, 1975; *Coffey et al.*, 1981; *Girard et al.*, 1982; *Williams et al.*, 1982; *Karcher et al.*, 1988; *Toon et al.*, 1992; *Pfeilsticker et al.*, 1997] and satellite [e.g., *Gille and Russell*, 1984; *Austin et al.*, 1986; *Russell et al.*, 1988;

Roche et al., 1994] data and is attributed to increasing photochemical destruction at lower latitudes.

One of the most striking features of Plates 1 and 2 is the existence of a pronounced seasonal cycle in HNO_3 at the higher latitudes in both hemispheres, whereas the seasonal cycle at lower latitudes is much weaker. Consistent with the seasonal patterns, although a high degree of longitudinal variability is evident in the high-latitude HNO_3 during winter, these variations are greatly reduced in spring and summer and are insignificant at low latitudes at all times of year. The seasonal dependence of the HNO_3 abundances at high latitudes, with a winter maximum and a summer minimum, has been described previously by *Lazrus and Gandrud* [1974], *Murcray et al.* [1975], *Coffey et al.* [1981], *Austin et al.* [1986], *Roche et al.* [1994], *Gille et al.* [1996], *Notholt et al.* [1997], and *Slusser et al.* [1998], among others. The smaller-amplitude seasonal dependence in HNO_3 at midlatitudes has been discussed by *Rinsland et al.* [1991] and *Jones et al.* [1994].

The strong seasonal cycle in 465-K HNO_3 mixing ratios at higher latitudes, and its absence at lower latitudes, arises from a combination of factors. Normally, the distribution of HNO_3 is determined by gas-phase processes: production by three-body recombination of OH and NO_2 and loss through photolysis and reaction with OH. However, other processes come into play in the low-sunlight conditions of the wintertime middle and high latitudes, where the photochemical lifetime of HNO_3 exceeds a month [*Austin et al.*, 1986]. Several investigators have noted that conventional gas-phase photochemical/dynamical models failed to accurately simulate the wintertime enhancement of HNO_3 at middle and high latitudes in the lower stratosphere observed in balloon [*Evans et al.*, 1985] and satellite [*Austin et al.*, 1986; *Jackman et al.*, 1987; *Hofmann and Solomon*, 1989; *Rood et al.*, 1990, 1993] measurements. These studies postulated the existence of a fast heterogeneous source of HNO_3 operating in and near the region of polar night in the lower stratosphere, such as the hydrolysis of N_2O_5 on background sulfate aerosol. Laboratory experiments [*Reihs et al.*, 1990] have indicated that this reaction produces gaseous HNO_3 even under conditions of enhanced sulfate

aerosol loading. Heterogeneous conversion of N_2O_5 to HNO_3 on sulfate aerosols (or on PSCs, followed by evaporation) has also been invoked to explain large column HNO_3 abundances in the Arctic measured by airborne [*Mankin et al.*, 1990; *Toon et al.*, 1992; *Blom et al.*, 1995] and ground-based [*Notholt et al.*, 1997; *Slusser et al.*, 1998] instruments. Similarly, *Keys et al.* [1993] and *Van Allen et al.* [1995] argued that observed increases in ground-based HNO_3 column amounts during autumn in Antarctica are attributable to N_2O_5 conversion on background aerosols.

This process may be particularly important at slightly higher altitudes, but it also has a strong influence on 465-K HNO_3 mixing ratios, both directly and through dynamical effects. As the polar regions fall into darkness after the autumnal equinox, radiative processes rapidly cool the polar stratosphere, the vortex spins up, and strong downward motion over this area begins [*Schoeberl and Hartmann*, 1991]. During late autumn and early winter, the lower stratospheric vortex is characterized by strong diabatic descent but very little latitudinal mixing across its boundary [*Manney et al.*, 1994b]. The descending air carries with it the chemical composition of regions higher in the stratosphere; since the peak of the HNO_3 profile is located at higher altitudes (~25 km, ~30 hPa), high HNO_3 concentrations in the interior and strong HNO_3 gradients at the edge of the vortex develop at 465 K as the vortex strengthens. This sharp increase in HNO_3 across the vortex boundary has been clearly demonstrated in aircraft column measurements [e.g., *Toon et al.*, 1992; *Blom et al.*, 1994, 1995] and also other satellite measurements [*Roche et al.*, 1994]. As is evident in the maps of Plates 1 and 2, in the absence of other effects such as PSC formation, high HNO_3 values correspond closely with high PV values and are excellent indicators of vortex size and shape.

Thus the photochemical conditions in the region of polar night (decreased HNO_3 photolysis and increased N_2O_5 being converted into HNO_3) combined with enhancement via diabatic descent lead to a wintertime maximum in HNO_3 at middle and high latitudes. In contrast, continuous photolysis during polar summer leads to very low HNO_3 concentrations. The lower latitudes do not experience the effects of either polar night/day or unmixed vertical

transport of air with higher HNO_3 mixing ratios from above, and consequently the HNO_3 seasonal cycle there is minimal.

HNO_3 mixing ratios at 465 K in the winter polar regions are primarily controlled by meteorological conditions: the strength of the diabatic descent, the permeability of the vortex, and the extent and duration of low temperatures (which govern PSC formation). In the Arctic especially there is a high degree of interannual variability in the strength and longevity of the polar vortex [*Manney et al.*, 1994a; *Dahlberg and Bowman*, 1994; *Waugh and Randel*, 1998], the occurrence and persistence of low temperatures [e.g., *Zurek et al.*, 1996], and the frequency and duration of PSC activity [*Poole and Pitts*, 1994]. These factors produce a concomitantly large interannual variability in HNO_3 sequestration and removal. For example, in mid-December the morphology of HNO_3 changes considerably from year to year (Plate 2). For the most part, the northern hemisphere winters since the launch of UARS have been characterized by lower temperatures and a stronger, more isolated vortex in the lower stratosphere than in the majority of previous northern winters dating back to 1978 [*Zurek et al.*, 1996]. However, in some years the below-average temperatures and anomalously-strong vortex have not developed until later in the winter. In mid-December 1991, the lower-stratospheric PV gradients were fairly strong but the temperatures had not yet dropped below typical HNO_3 condensation values ($\sim$195 K or below) [*Zurek et al.*, 1996]; a combination of vertical transport, segregation of vortex from lower-latitude air, and lack of PSC events led to uniformly high HNO_3 mixing ratios throughout the vortex interior. Although 465-K temperatures and PV gradients in mid-December 1992 were similar to those of 1991 [*Zurek et al.*, 1996], HNO_3 mixing ratios inside the vortex were not as uniformly high. The 1994–95 early winter was unusually cold, with 465-K temperatures hovering near the type II PSC formation threshold by mid-December [*Zurek et al.*, 1996], and HNO_3 was substantially depleted in the low-temperature region. The 1996–97 early winter was unusually warm, with an extremely weak vortex in the lower stratosphere [*Coy et al.*, 1997], and in mid-December the high HNO_3 abundances arising from transport were still being diluted

through mixing of HNO_3-poor air from low latitudes into the vortex.

Much less interannual variability in vortex evolution occurs in the southern hemisphere, particularly in the early winter [*O'Neill and Pope*, 1990; *Waugh and Randel*, 1998]. As a consequence, the HNO_3 behavior is fairly consistent every year (Plate 1). Although the location of the cold region in mid-June varies from year to year, the overall pattern of a confined area of severely-depleted gas-phase HNO_3 coincident with the lowest temperatures and banded by high HNO_3 values inside a relatively well-developed vortex occurs in every year. The HNO_3 morphology is even more uniform from year to year in late-August. The general picture of a "core" characterized by low HNO_3 values and small latitudinal gradients surrounded by a "collar" characterized by high HNO_3 values and large latitudinal gradients was first described by *G. Toon et al.* [1989] *Toon et al.* [1989a] from aircraft column measurements and is also evident in UARS CLAES data [*Roche et al.*, 1994].

Little year-to-year variation is expected in the summertime HNO_3 distribution, which in general is determined by gas-phase photochemistry as described above. However, several modeling studies [e.g., *Hofmann and Solomon*, 1989; *Brasseur and Granier*, 1992] have demonstrated the potential for the heterogeneous hydrolysis of N_2O_5 to cause substantial increases in HNO_3 abundances under conditions of enhanced sulfate aerosol loading following large volcanic eruptions. Profiles of HNO_3 measured at both northern [*Webster et al.*, 1994] and southern [*Rinsland et al.*, 1994] midlatitudes after the Mount Pinatubo eruption compare much better with models that include this reaction. It is possible that the decline in HNO_3 concentrations after 1993 apparent in the maps for mid-January (Plate 1) and, to a lesser extent, for mid-July (Plate 2) is related to the slow decay of the Pinatubo aerosol cloud. This is consistent with the gradual decreases in ground-based HNO_3 column amounts that have been observed at southern midlatitudes [*Koike et al.*, 1994] and northern low [*David et al.*, 1994] and high [*Slusser et al.*, 1998] latitudes as the stratosphere recovered from Pinatubo-induced HNO_3 enhancement. *Kumer et al.* [1996] also reported a distinct decreasing trend in UARS CLAES HNO_3 abundances, especially in the southern hemisphere, and attributed it to the

diminishing influence of heterogeneous reactions as the Pinatubo aerosols settled out. We too have observed decreasing trends in the MLS HNO_3 abundances at midlatitudes, a more detailed analysis of which is beyond the scope of this paper. The trends in the MLS midlatitude data have also been discussed by *Randel et al.* [1998] (W. J. Randel et al., Space-time patterns of trends in stratospheric constituents derived from UARS measurements, submitted to *Journal of Geophysical Research*, 1998).

3.2. Climatological Fields

To explore the interhemispheric differences in synoptic behavior more generally, we have produced "climatological" HNO_3 fields from the days represented in Plates 1 and 2. Again, each yaw period has at least 4 and at most 6 years represented. Thus, for example, the mid-December climatology is derived by averaging together 6 days of data, and the mid-July climatology is derived by averaging together 4 days of data. Possibly a more traditional approach to establishing climatologies would have been to average together all of the available days in a given month; however, this approach would have biased the results toward the earlier years, since the data sampling in later years has become quite sparse. Thus we have chosen to create the climatologies from a single day in each year where available. The climatological fields are shown in Plate 3 for both the southern and northern hemispheres. In addition to averaging together the MLS HNO_3 data for these days, we have also averaged the temperature and the PV fields from the UKMO analyses. These contours are overlaid on the climatology maps as they were on the maps for individual days.

Comparison of the early-April and early-October climatologies (Plate 3) indicates a slightly higher degree of organized descent down to the 465-K level at the beginning of winter in the southern hemisphere than in the northern hemisphere, where in many years a summertime HNO_3 morphology still persists at this time (see Plate 2). In the southern hemisphere, the largest differences from the climatology (not shown) occur in 1992, the year for which the vortex was the most well-developed this early in the winter season.

In general, in the southern hemisphere the June and August data exhibit the largest deviations from their respective climatologies, reflecting significant interannual differences in PSC formation and distribution. Since these deviations from climatology can be difficult to track by eye, we include a plot for the mid-June deviations in Plate 4. At the 465-K level in mid-June, the vortex is still wobbly, the area of low temperatures is still fairly confined, and the location of the cold region can vary from one side of the pole to the other; consequently, the deviations from climatology are large in every year, with maximum deviations occurring in the collar region on any given day. Similarly, in late-August the extensive cold regions are not quite concentric with the vortex, and small variations from year to year in where the collar and the denitrified regions adjoin also lead to large deviations from the climatological values (not shown).

A parallel situation is seen in the northern hemisphere, with large interannual differences in PSC activity again leading to the largest deviations from their respective climatologies in the winter months of December and February (not shown). In addition, the Arctic vortex is subject to considerable distortion through planetary wave activity and in any given year is therefore likely to be centered off the pole and highly elongated; thus even years with similar temperature/PSC conditions may display large differences in the locations of high HNO_3 values. While gas-phase HNO_3 loss is neither severe nor widespread in late-February in any year, the climatology (Plate 3) does exhibit lower HNO_3 mixing ratios in the preferred PSC formation regions in the corridor between Greenland and Scandinavia, and in the area poleward of Scandinavia.

That the wintertime behavior of HNO_3 is distinctly different in the two hemispheres is clearly illustrated by comparison of the late-August and early-November climatologies in the southern hemisphere with the late-February and late-April climatologies in the northern hemisphere. Because MLS is sensitive to HNO_3 only in the gas-phase, the deficit in late-August, when 465-K temperatures in every year were still low enough for PSCs to continue sequestering HNO_3, is not in itself proof of denitrification. However, by early-November the

temperatures in all years had warmed well above PSC existence thresholds. The strength of the PV gradients in November, as indicated in the maps in Plate 1 (and in the averaged PV field in Plate 3), implies that the vortex was still intact at 465 K, inhibiting mixing between polar and midlatitude air. Therefore, we interpret the enduring depression in gas-phase HNO_3 over Antarctica in November to be evidence of denitrification. In contrast, although gas-phase HNO_3 loss is observed on individual days in the Arctic, it is less intense, more localized, and more transient, with no suggestion of significant denitrification in the late-February climatology. This work extends the conclusions of *Santee et al.* [1995], which were based on MLS HNO_3 data from a single winter in both hemispheres.

Another disparity between the HNO_3 morphologies in the two hemispheres is that the peak mixing ratios attained during winter are larger in the Arctic. In the north, HNO_3 abundances are largest near the center of the vortex, where diabatic descent tends to be strongest [*Manney et al.*, 1994b]. In the south, they are largest in the collar region, both because the vortex core is severely denitrified and because the strongest descent in the lower stratosphere occurs along the vortex edge [*Manney et al.*, 1994b]. Although diabatic descent is more vigorous throughout the winter in the Arctic than in the Antarctic [*Manney et al.*, 1994b], in the southern hemisphere the effects of unmixed descent are visible at 465 K both earlier in the fall, since the vortex deepens more rapidly [*Manney and Zurek*, 1993] and provides a strong barrier to latitudinal mixing sooner than in the north, and later in the spring, since PV gradients remain strong and unmixed descent continues for a much longer period than in the north [*Manney et al.*, 1994b; *Abrams et al.*, 1996a, b]. Thus, in the absence of denitrification, the downward transport of HNO_3-rich air in a confined area over the course of the winter would be expected to produce HNO_3 mixing ratios at the 465-K level in the Antarctic as high as or higher than those in the Arctic. However, denitrification may affect HNO_3 abundances even in PSC-free regions, if transport processes inside the vortex lead to dilution of the high HNO_3 concentrations in unperturbed areas as denitrified air is mixed in.

Large-scale polar processing and ozone depletion cease with the breakup of the vortex

in late winter or early spring. Northern hemisphere winters in particular are distinguished by a large variation in the duration of a strong vortex in the lower stratosphere [*Manney et al.*, 1994a; *Dahlberg and Bowman*, 1994; *Waugh and Randel*, 1998]. Most commonly, the final warming occurs and the vortex dissipates in March, with small remnants of high PV persisting in the lower stratosphere into early April, after erosion of the main vortex [*Manney et al.*, 1994a, b; *Dahlberg and Bowman*, 1994; *Waugh and Randel*, 1998]. These lingering vortex fragments are evident in the late-April maps in Plate 2, illustrating that the correlation of HNO_3 with high PV values is maintained throughout the winter. In 1997, however, the vortex remained substantially intact in the lower stratosphere into early May, exhibiting unprecedented longevity [*Coy et al.*, 1997]. The unusually large vortex area in 1997 tends to bias the late-April climatology (Plate 3), which as a result is perhaps somewhat less representative of the typical situation than the other climatologies.

Finally, we find that the summertime HNO_3 distribution is very similar in both hemispheres (compare the mid-January and mid-July maps in Plate 3). In addition, in both hemispheres the summertime data exhibit the smallest deviations from their respective climatologies. For the Antarctic, the mid-January deviations are also shown in Plate 4. Despite the large deviations from climatology in every winter (exceeding ± 5 ppbv in mid-June and late-August), the summertime values are fairly small in every year. Even when expressed in terms of percentages (not shown), the midsummer deviations from climatology are considerably smaller than the midwinter values. Comparable deviations are seen for the Arctic in mid-July (not shown). The fact that the deviations are essentially similar in both hemispheres and in every year implies that, although there are large interhemispheric and interannual differences in the extent and duration of PSC activity and denitrification, the HNO_3 at high latitudes always recovers to about the same values.

4. Overview of Mean Evolution

We now explore the latitudinal, seasonal, interannual, and interhemispheric variations in HNO_3 through the use of zonal means rather than mapped data. In Plate 5 the MLS data points for each of the individual days in Plates 1 and 2 have been binned into 5° latitude bands and averaged. Again we see that HNO_3 abundances increase with latitude in all seasons and in both hemispheres and attain their maximum values in the polar regions during winter, except in areas of strong PSC activity and denitrification. Winters in the Arctic are characterized by large interannual variability, with the mixing ratios at the highest latitudes differing by up to a factor of 2 from year to year in mid-December and late-February. In the Antarctic, while there is significant interannual variability in the extent of HNO_3 sequestration in mid-June, in late-August in every year the HNO_3 mixing ratios are extremely low at the highest latitudes. However, a large degree of interannual variability does occur in the collar region in late-August, as is evident in Plate 1. Small differences from year to year at the highest latitudes in early-November and late-April reflect differences in the degree of denitrification and extent of residual vortex fragments in the southern and northern hemisphere, respectively. At all other latitudes and seasons the interannual variability is minimal ($\sim$2 ppbv or less).

4.1. Zonal Mean Time Evolution

Up to this point we have examined results from individual days. While this approach provides snapshots of the HNO_3 distribution in different seasons, it does not allow a detailed look at the HNO_3 evolution over the course of the year. To this end, in Plate 6 we show time series of 465-K MLS HNO_3 as a function of latitude over complete annual cycles, starting in early winter (April in the south, October in the north) each year. Because the Arctic vortex is more distorted and less concentric with latitude circles than the Antarctic vortex, zonal means of this kind are less representative of actual vortex behavior in the north; nevertheless, it is still instructive to compare the progression of zonal-mean HNO_3 values in the two hemispheres. In general, differences in the development of high vortex HNO_3 at 465 K are relatively small at

the very beginning of winter, but the behavior in the two hemispheres diverges as the season proceeds. By about May 20 in the south and November 20 in the north (50 days after the start of the plots), the gradients in the high-latitude HNO_3 have become steeper in the south, where the stronger vortex provides a more effective barrier to mixing with lower-latitude air, than in the north, where the vortex is less zonally symmetric. Although severe denitrification (HNO_3 < 3 ppbv) is never apparent in the north, it starts to become evident on about June 20 (80 days after the start of the plot) every year in the south. The precise end of the effects of severe denitrification has not been captured in the data in most years, but the zonal mean values at the highest latitudes have typically begun to recover to values > 3 ppbv by the last week in October (210 days after the start of the plot), except in the last two years of measurements.

Zonal-mean climatological fields, shown in Plate 7, were produced by averaging together the results for the individual years. Because a particular UARS month starts about 5 days earlier in each succeeding year (see section 2.1), the data gaps between the south-looking (top) or north-looking (bottom) UARS months are shortened when several years of measurements are averaged together; "edge effects" arise at the month boundaries where data from fewer years contribute to the average. These climatologies encapsulate the general patterns of HNO_3 behavior discussed above and in section 3.

Next, we evaluate the extent of interannual and interhemispheric differences in the HNO_3 seasonal cycle by examining daily means calculated in various latitude bands. Results for both hemispheres are shown in Plate 8, where the data have been binned into 5° latitude bands and averaged. As discussed in the previous section, the amplitude of the seasonal cycle diminishes toward the equator, with a seasonal signature of only $\sim$2 ppbv present in the zonal means for the 40–45° bands. Even weaker seasonal cycles are seen at lower latitudes (not shown). At middle and low latitudes the seasonal maxima and minima occur during the winter and summer months, respectively, in each hemisphere.

At the lower latitudes, the interannual variability at a given time of year appears to be comparable to the seasonal variation for a given year ($\sim$2 ppbv or less). However, assessment

of the year-to-year variability is complicated by the fact that the data display a yaw-cycle dependence, whereby mixing ratios tend to be larger in the middle than at the beginning or end of a UARS month. Similar artifacts have been noted in some aspects of the MLS temperature [*Fishbein et al.*, 1996], ozone [*Froidevaux et al.*, 1996], and water [*Lahoz et al.*, 1996] retrievals. Thus, care must be taken to compare data from different years at corresponding points in the yaw periods. In addition, some of the differences between years that appear to arise from interannual variability may actually be associated with Pinatubo effects, as mentioned above. The fact that only minor differences were found between profiles obtained at the same time of year by LIMS in 1979 and the ATMOS experiment on Spacelab 3 in 1985 at 47°S and 29°N also led *Russell et al.* [1988] to conclude that interannual variations at these latitudes are small.

The amount of interannual variability is somewhat larger at southern high latitudes, where the more well-developed vortex in early-April 1992 is reflected in higher average HNO_3 mixing ratios and where different degrees of PSC development affect the early-June values. Despite these early-winter differences, in every year severe HNO_3 depletion has occurred by July in the 75–80°S and 70–75°S bands. By the beginning of the next south-viewing period in early- to mid-August, the very low HNO_3 abundances have begun to rebound; they continue to increase into the following south-viewing period in early- to mid-November. By the end of that period, HNO_3 concentrations have returned to their summertime values and remain essentially constant through January before beginning to increase again in the austral fall (mid- to late-March). The patterns of HNO_3 loss and recovery are similar, although less dramatic, in the 65–70°S band.

Northern high latitudes display an even greater degree of interannual variability. Mid-December HNO_3 abundances were large in 1991, when the lower-stratospheric vortex was strong but temperatures were relatively high [*Zurek et al.*, 1996], and small in 1996, when the lower-stratospheric vortex was weak [*Coy et al.*, 1997]. HNO_3 levels remained high in March in 1992 and 1994, after relatively warm winters, but dropped considerably in 1995

after an unusually cold winter [*Zurek et al.*, 1996]. We will discuss the comparisons between the zonal mean behavior in the two hemispheres, and their implications, in more detail in section 4.3.

4.2. The Antarctic Winter Polar Vortex

Of course, looking at zonal means is problematic at high latitudes during winter because, as discussed earlier, HNO_3 is strongly correlated with the polar vortex, which is not concentric with latitude circles even in the southern hemisphere. Therefore, in Plate 9 we show HNO_3 averaged within PV contours representative of Antarctic vortex "inner core" and "collar" regions at the 465-K level. The two regions do not abut. The collar region was delimited by $0.25 \times 10^{-4}\ \mathrm{K\,m^2\,kg^{-1}\,s^{-1}} < \mathrm{PV} < 0.40 \times 10^{-4}\ \mathrm{K\,m^2\,kg^{-1}\,s^{-1}}$, where the outermost contour represents a typical definition of the vortex edge during winter and coincides with a strong barrier to mixing [*Manney et al.*, 1994b] and the innermost contour was chosen to generally encompass the region of high HNO_3 along the vortex rim. In selecting the inner core boundary criterion, $\mathrm{PV} > 0.48 \times 10^{-4}\ \mathrm{K\,m^2\,kg^{-1}\,s^{-1}}$, a balance had to be struck between a contour that was well poleward of the collar region and one that maintained its identity into the spring. Note that averages over the vortex inner core region are also averages over an annulus, since MLS data coverage does not extend poleward of ~80°. UKMO average and minimum temperatures in these regions are also shown. We focus here on the three years (1992–1994) for which MLS data sampling is most continuous, although data for the other years are included for completeness.

As seen in the highest-latitude zonal means (Plate 8), the vortex inner-core average mixing ratios drop sharply in early June; measured values in this region are very low by late-June/early-July, when average temperatures fall below 188 K. The correlation of the HNO_3 behavior with temperature during this time period, and its implications for PSC phase and composition, is explored in detail in *Santee et al.* [1998]. The results of Plate 9 suggest that HNO_3 abundances in the vortex inner core increase slightly sometime during the

mid-winter gap between south-looking observing periods. They then continue to increase at least into September, if not later. Thus the HNO_3 at 465 K already shows signs of recovery in mid-winter, even though temperatures at this level are still quite low. We will return to this point below.

Consistent with these indications of mid- to late-winter HNO_3 replenishment, *Toon et al.* [1989a] reported a significant increasing trend in the HNO_3 burden in the vortex core throughout September 1987 and suggested either evaporation of frozen forms as the vortex warmed or descent as possible explanations. Similarly, measurements by *Coffey et al.* [1989] also showed a small increase in HNO_3 vertical column amounts inside the vortex during September 1987. More recently, 1992 UARS CLAES data at 46 hPa also suggest a small increase in zonal-mean HNO_3 mixing ratios in the 72–80°S band from mid-August to mid-September, followed by recovery to summertime values by the end of November [*Roche et al.*, 1994]. On the other hand, HNO_3 column amounts over Arrival Heights (78°S) presented by *Keys et al.* [1993] exhibited no particular trend from the end of August until mid-October, 1991, after which an increase was observed that was partially attributed to the evaporation of remaining PSCs and to meridional mixing during vortex breakup. In addition, *Klein et al.* [1996] saw no change in the HNO_3 content at 19 km over McMurdo Station (78°S) during the period from September 4 to October 8, 1994.

Two sets of ground-based measurements provide information about the seasonal variations in HNO_3 over the South Pole. *Van Allen et al.* [1995] report total HNO_3 column abundance over an 11-month period from mid-January to mid-November 1992, although HNO_3 could be retrieved on only 18 days in all during this period. They observed a trend to higher HNO_3 column amounts in March 1992, with high values persisting through June 9; a sharp decline occurred between that date and the next HNO_3 retrieval on June 27. HNO_3 column values then continued to fall in July. No HNO_3 retrievals were reported by *Van Allen et al.* [1995] for August or September 1992, but a single measurement at the beginning of October suggested no change in the total HNO_3 column over the South Pole from that

observed at the end of July, and measurements in mid-October and mid-November implied that the HNO_3 column had recovered to only about 50% of the summertime (January/February) values.

de Zafra et al. [1997] present South Pole HNO_3 vertical profiles and column densities over the range from ~15 to 48 km for a 9-month period from mid-April 1993 to mid-January 1994, although in this case measurements were made on only 63 days altogether. They observed a small increase in the peak mixing ratio (at ~23–24 km) between the start of their 1993 observations in mid-April and late May, which they interpret as the final stage of a more pronounced increase that occurred earlier in the fall. Although not fully comparable, the 1993 465-K MLS vortex inner-core averages (and zonal means in the 75–80°S band) and the *de Zafra et al.* [1997] South Pole data exhibit very good agreement, in both the timing and the magnitude of HNO_3 decreases. *de Zafra et al.* [1997] report HNO_3 mixing ratios at 20 km of ~11 ppbv in mid-May just prior to the onset of depletion, dropping to <0.5 ppbv by early July. However, although the 1993 data of *de Zafra et al.* [1997] indicated that the HNO_3 mixing ratios at 20 km (as well as the integrated column densities) over the South Pole began to rebound in late-August, the recovery was slow. HNO_3 abundances continued to increase throughout the spring, reaching 4.5 ppbv in mid-December, after which they briefly leveled off; the last few days of data in mid-January 1994 showed that HNO_3 values were again beginning to rise. Comparison of the South Pole data with the MLS data in the vortex inner core suggests that HNO_3 replenishment over the pole starts later and progresses more slowly than that at slightly lower latitudes.

In discussing the observed slow increase in HNO_3 in the lower stratosphere during the spring/summer period, *de Zafra et al.* [1997] note that evaporation of any PSCs remaining when temperatures rise above PSC existence thresholds toward the end of winter would result in an immediate release of HNO_3 and rapid increase in gas-phase abundances. Since heterogeneous reactions on PSCs can serve as a source for HNO_3, an excess of HNO_3 could then persist for several weeks until HNO_3 photolysis reestablished photochemical equilibrium.

de Zafra et al. [1997] conclude that gravitational settling of the particles removed the HNO_3 to lower altitudes where, even if released back to the gas phase, it could not be detected by their instrument.

Interestingly, the MLS data indicate increasing HNO_3 mixing ratios at 465 K while temperatures at that level remain low. However, it must be borne in mind that the combined effects of denitrification and dehydration alter the PSC existence thresholds as winter progresses. For example, assuming 12 ppbv of HNO_3 and 4.5 ppmv of H_2O at 50 hPa, the existence thresholds for water ice and nitric acid trihydrate (NAT, using the formula of *Hanson and Mauersberger* [1988]) PSCs are ~188 K and ~195 K, respectively. In the wake of severe denitrification/dehydration, assuming 1 ppbv of HNO_3 and 2.5 ppmv of H_2O at 50 hPa (based on MLS data in mid-August), the existence thresholds for water ice and NAT PSCs drop to ~185 K and ~190 K, respectively. In Plate 9 we compare the MLS HNO_3 measurements to UKMO temperatures in light of these estimated PSC existence thresholds. Comparisons of this kind are necessarily limited by the uncertainties associated with each data set. *Manney et al.* [1996b] found that systematic biases between the UKMO temperatures and radiosonde observations at 50 hPa at high southern latitudes were less than 1 K throughout the winter, although differences on individual days can be much larger.

During the UARS years, average 465 K temperatures in the vortex inner core typically stop decreasing in mid-July, with the lowest values at or just below 185 K. Because of a combination of yaw maneuvers and data outages, MLS never observed the southern vortex between mid-July and early-August. By the beginning of the next MLS observing period, the average temperatures have risen above 185 K (to ~188 K in 1992–1994). It is possible that the increase in average temperature above the 185 K level triggers the evaporation of any remaining water ice PSCs. Since these PSCs can also incorporate HNO_3 vapor, either through the simultaneous cocondensation of HNO_3 and H_2O molecules during ice growth or as NAT particles that serve as condensation nuclei for ice crystals [*Toon et al.*, 1989b; *Turco et al.*, 1989], this mechanism could be responsible for the initial release of HNO_3 between observing

periods hinted at by the MLS data.

Throughout the August/September observing period, the HNO_3 mixing ratios are strongly correlated with temperature in the vortex inner core region. In addition to exhibiting an overall increasing trend with temperature, the HNO_3 also fluctuates with small temperature changes. This is apparently true even when temperatures are slightly above 190 K. Caution must be exercised with this interpretation, however, since occasionally the PV gradients become sufficiently strong that the contour defining the vortex "inner core" actually clips the collar region of high HNO_3; this effect, coupled with larger collar-region abundances than in other years (see Plate 1), is at least partially responsible for the step up in average HNO_3 mixing ratios in mid-August 1994 and for the consistently higher average HNO_3 values in late-August 1996. Nevertheless, the rapidity of the HNO_3 rebound during this period of generally rising (though still low) temperature and the fact that HNO_3 continues to display variations with temperature suggest that the lower stratosphere has not been completely denitrified through particle sedimentation even in late winter. In addition, small temperature decreases can still lead to HNO_3 depletion through renewed PSC formation. Measurements of aerosol extinction by CLAES also demonstrate that intermittent localized PSC events continue to occur at 465 K until at least mid-September [*Santee et al.*, 1996a; *Mergenthaler et al.*, 1997], and measurements of aerosol extinction at high southern latitudes by the Polar Ozone and Aerosol Measurement (POAM) II solar occultation instrument indicate the occurrence of PSCs at the 20-km level as late as mid-October [*Fromm et al.*, 1997].

Alternatively, the HNO_3 replenishment may arise through dynamical processes. Although either mixing of the denitrified and the collar regions inside the vortex or mixing of midlatitude air deep into the vortex would increase HNO_3 abundances in the Antarctic vortex inner core, calculations have shown that neither of these processes operates to a significant degree prior to the breakup of the vortex much later in the spring [e.g., *Schoeberl et al.*, 1992; *Bowman*, 1993; *Manney et al.*, 1994b]. That HNO_3 abundances in the collar region remain relatively constant and enhanced throughout the winter season (Plate 9) implies that the core and the

collar regions stay essentially separate and thus also argues against a substantial amount of large-scale horizontal mixing.

A more plausible dynamical explanation for the observed HNO_3 increase starting in August is diabatic descent bringing air with higher HNO_3 concentrations down to the 465-K level. Although the uncertainties are large, trajectory calculations by *Manney et al.* [1994b] have indicated that, in the southern hemisphere, air parcels in the lower stratosphere continue to descend until mid-October and most of the parcels at the 465-K level remain confined inside the vortex (or its remnants) until mid-December. Similar conclusions have been reached from observational studies of long-lived tracers [*Crewell et al.*, 1995; *Abrams et al.*, 1996a]. Therefore ongoing descent probably contributes to HNO_3 increases at 465 K into the spring, with its effect diminishing in late winter as the descent rate becomes small. However, a rough estimate based on MLS data suggests that a vortex-averaged descent rate on the order of 1–2 K/day would be necessary throughout the late-winter period to sustain the observed HNO_3 increase. As this value is unrealistically large [e.g., *Manney et al.*, 1994b], descent cannot be solely responsible for the HNO_3 recovery, nor would it be expected to be so closely correlated with small temperature variations.

We conclude that renitrification at 465 K is likely achieved through a combination of PSC evaporation and continuing weak diabatic descent. Full understanding of the HNO_3 mixing ratios in the southern hemisphere late winter/early spring requires extensive modeling efforts, beyond the scope of this study, to characterize and quantify the simultaneous (and, in some cases, competing) effects of PSC evaporation, recurring PSC formation, continuing heterogeneous reactions on PSC particles and background sulfate aerosols (a potential source of HNO_3), permanent removal through gravitational settling of PSC particles, vertical transport, horizontal mixing, and photodissociation, although the current levels of uncertainty in both models and data compared to the relatively small changes shown in Plate 9 may preclude a definitive budget analysis at this time.

4.3. Interhemispheric Comparisons

Returning to Plate 8, overlaid on the northern hemisphere plot is a black line representing the daily averages calculated from the southern hemisphere data points in every year. This allows the very dissimilar progression of the high-latitude HNO_3 in the two hemispheres to be compared. Although the early-winter tendency is similar in both hemispheres, the steep decreasing trends in the 75–80°S and 70–75°S bands in June stand in strong contrast to the behavior in the 75–80°N and 70–75°N bands in December, when the HNO_3 is still high or even increasing through the action of diabatic descent. Whereas in the Antarctic the HNO_3 mixing ratios increase from August to November as they recover from severe denitrification, in the Arctic they decrease from March through May. A similar decreasing trend was seen in vortex-averaged HNO_3 at 465 K by *Santee et al.* [1997]. Since this gradual reduction in HNO_3 mixing ratios in the north takes place even in years when PSC activity is minimal, continues well past the time of ongoing PSC activity in every year, and occurs during the corresponding recovery period in the south, it is unlikely to be related to denitrification. Rather, it probably results from increased amounts of sunlight leading to a greater degree of HNO_3 photolysis in combination with enhanced mixing of vortex and lower-latitude air as the vortex erodes. Again, a more definitive answer must await detailed modeling of HNO_3 photochemistry and transport processes. By the end of November (May) in the south (north), the zonal-mean HNO_3 abundances at the highest latitudes are once again in agreement in the two hemispheres.

The wintertime disparity between the two hemispheres is also significant in the 65–70° band. However, the results for the two hemispheres are virtually indistinguishable for the 60–65° band and the bands equatorward, even during the winter months. This has several implications. One is that the amount of mixing between denitrified and unperturbed air is relatively small in the outer portion of the vortex (at least in the zonal mean), since otherwise a higher degree of inconsistency would be expected between the north and the south. Similar arguments were made on the basis of MLS H_2O data by *Morrey and Harwood* [1998]. The conclusion that little mixing occurs inside the vortex is also consistent with the calculations of

Schoeberl et al. [1992] and *Bowman* [1993].

Another inference that can be drawn from the results of Plate 8 is that the effects of severe denitrification are confined in both space and time to the regions poleward of 65°S during the winter and early spring. This result is contrary to the conclusions of *Tuck et al.* [1994], who used the correlation between NO_y (total reactive nitrogen) and N_2O measured during both Arctic and Antarctic aircraft campaigns to argue for the significant spread of denitrification from the vortex to midlatitudes above 400 K during winter. A recent analysis by *Keim et al.* [1997], again based on NO_y/N_2O correlations from aircraft measurements, also found little evidence that export of denitrified air from the vortex influenced the midlatitude NO_y budget above 400 K during the winter.

The agreement between northern and southern hemisphere HNO_3 abundances in the 60–65° and 55–60° bands (and equatorward) shown in Plate 8 implies that the global impact of severe denitrification is minimal, at least over the large spatial scales represented in zonal means. This is true not only during the winter, but after the breakup of the vortex as well. HNO_3 mixing ratios increase through the winter in both hemispheres at these latitudes, presumably through diabatic descent and/or heterogeneous reactions on sulfate aerosols, and then begin to decrease in the spring. That the decrease in midlatitude zonal-mean HNO_3 abundances in spring follows the same trend in both hemispheres argues against a substantial role for the mixing in of denitrified air as the vortex dissipates, since the north does not experience widespread intense denitrification. Of course, this process could affect local HNO_3 abundances on spatial scales not discernable in the zonal-mean values (or indeed in the MLS data at all). It is more likely that the springtime decrease observed in the midlatitude zonal-mean mixing ratios is related to the increasing HNO_3 photolysis rate. Furthermore, at the highest latitudes, where Antarctic denitrification is most severe, zonal-mean HNO_3 abundances recover to similar values at the end of every winter in both hemispheres. Thus even at the latitudes where denitrification actually occurs it has no long-term large-scale influence beyond the winter and early-spring period when the vortex is still largely intact.

5. Summary and Implications

We examined measurements of gas-phase HNO_3 made by the UARS MLS instrument through six complete annual cycles in both hemispheres. To provide an overview of the seasonal, interhemispheric, and interannual variations in the distribution of HNO_3 in the lower stratosphere, we presented maps at 465 K for selected days in each of the 5 north-looking and 5 south-looking MLS observing periods in each year. Climatological fields representative of the different seasons were then constructed by averaging together the data from the individual days in each year. The zonal mean evolution was explored through time series of MLS HNO_3 at 465 K as a function of latitude over complete annual cycles; again, zonal-mean climatological fields were derived by averaging together the results for the individual years. The extent of interannual and interhemispheric differences in the HNO_3 seasonal cycle was then investigated by calculating daily means from data binned into 5° latitude bands between 40° and 80° in both hemispheres. Because HNO_3 is strongly correlated with the polar vortex during winter, averages of HNO_3 calculated within PV contours representative of vortex "inner core" and "collar" regions at the 465-K level were also shown for the southern hemisphere.

Consistent with many previous studies (see section 3), the MLS HNO_3 data display a large variation with latitude and a pronounced seasonal cycle at middle and high latitudes in both hemispheres, whereas the seasonal cycle at lower latitudes is much weaker. The MLS data reveal that, outside of the winter polar regions, zonal-mean HNO_3 mixing ratios are comparable in the two hemispheres in all corresponding latitude bands and in all years examined. Except at high latitudes, interannual variability is minimal, and there does not appear to be a significant hemispheric asymmetry in the overall HNO_3 distribution or its seasonal cycle.

Because HNO_3 mixing ratios at 465 K in the winter polar regions are primarily controlled by meteorological conditions (the strength of the diabatic descent, the permeability of the vortex, the extent and duration of low temperatures), they exhibit a large degree of interannual variability, particularly in the Arctic. Although the early-winter trends are similar in the north

and the south, the HNO_3 behavior diverges in the two hemispheres as winter progresses. In general, the peak HNO_3 mixing ratios attained during winter are larger in the Arctic than in the Antarctic. Significant interhemispheric differences in PSC activity lead to distinctly different patterns of HNO_3 depletion, with the Antarctic experiencing widespread severe denitrification while the gas-phase HNO_3 loss in the Arctic is less intense, more localized, and more transient. However, the MLS data indicate that denitrification is not complete even in the Antarctic. The rapidity of the recovery in HNO_3 abundances during the mid- to late-winter period (when temperatures, though still low, are generally rising) and the fact that HNO_3 continues to fluctuate with small changes in temperature suggest that not all PSC particles sediment out of the lower stratosphere. We conclude that renitrification at 465 K is most likely achieved through a combination of PSC evaporation and continuing weak diabatic descent.

Despite the large interhemispheric and interannual differences in the extent and duration of PSC activity and denitrification, the zonal-mean HNO_3 abundances at the highest latitudes are once again in agreement in the two hemispheres by the end of November (May) in the south (north). Thus the HNO_3 recovers to similar values at the end of every winter and in both the Arctic and the Antarctic. Furthermore, the averaged HNO_3 values for the two hemispheres are virtually indistinguishable for latitudes equatorward of 65°, even during the winter months. This implies that the effects of severe denitrification are confined in both space and time to the regions poleward of 65°S during the winter and early spring. We conclude that, at least in a zonal mean sense, denitrification does not have a strong influence on midlatitudes, either during or after the winter, nor does it have a long-term impact at high latitudes; that is, there is no "memory" from one winter to another.

Acknowledgments. We thank A. Tabazadeh for helpful comments and the UKMO (R. Swinbank and A. O'Neill) for meteorological analyses. Work at the Jet Propulsion Laboratory, California Institute of Technology, was done under contract with the National Aeronautics and Space Administration.

References

Abrams, M. C., et al., ATMOS/ATLAS–3 observations of long-lived tracers and descent in the Antarctic vortex in November 1994, *Geophys. Res. Lett.*, *23*, 2341–2344, 1996a.

Abrams, M. C., et al., Trace gas transport in the Arctic vortex inferred from ATMOS ATLAS–2 observations during April 1993, *Geophys. Res. Lett.*, *23*, 2345–2348, 1996b.

Andrews, D. G., Some comparisons between the middle atmosphere dynamics for the southern and northern hemispheres, *Pure and Appl. Geophys.*, *130*, 213–232, 1989.

Austin, J., R. R. Garcia, J. M. Russell, III, S. Solomon, and A. F. Tuck, On the atmospheric photochemistry of nitric acid, *J. Geophys. Res.*, *91*, 5477–5485, 1986.

Barath, F. T., et al., The Upper Atmosphere Research Satellite Microwave Limb Sounder Instrument, *J. Geophys. Res.*, *98*, 10,751–10,762, 1993.

Blom, C. E., H. Fischer, N. Glatthor, T. Gulde, and M. Höpfner, Airborne measurements during the European Arctic Stratospheric Ozone Experiment column amounts of HNO_3 and O_3 derived from FTIR emission sounding, *Geophys. Res. Lett.*, *21*, 1351–1354, 1994.

Blom, C. E., H. Fischer, N. Glatthor, T. Gulde, M. Höpfner, and C. Piesch, Spatial and temporal variability of $ClONO_2$, HNO_3, and O_3 in the Arctic winter of 1992/1993 as obtained by airborne infrared emission spectroscopy, *J. Geophys. Res.*, *100*, 9101–9114, 1995.

Bowman, K. P., Large-scale isentropic mixing properties of the Antarctic polar vortex from analyzed winds, *J. Geophys. Res.*, *98*, 23,013–23,027, 1993.

Brasseur, G., and C. Granier, Mount Pinatubo aerosols, chlorofluorocarbons and ozone depletion, *Science*, *257*, 1239–1242, 1992.

Brune, W. H., J. G. Anderson, D. W. Toohey, D. W. Fahey, S. R. Kawa, R. L. Jones, D. S. McKenna, and L. R. Poole, The potential for ozone depletion in the Arctic polar stratosphere, *Science*, *252*, 1260–1266, 1991.

Coffey, M. T., W. G. Mankin, and A. Goldman, Simultaneous spectroscopic determination of the latitudinal, seasonal, and diurnal variability of stratospheric N_2O, NO, NO_2, and HNO_3, *J. Geophys. Res.*, *86*, 7331–7341, 1981.

Coffey, M. T., W. G. Mankin, and A. Goldman, Airborne measurements of stratospheric constituents over Antarctica in the Austral spring, 1987. 2. Halogen and nitrogen trace gases, *J. Geophys. Res.*, *94*, 16,597–16,613, 1989.

Coy, L., E. R. Nash, and P. A. Newman, Meteorology of the polar vortex: Spring 1997, *Geophys. Res. Lett.*, *24*, 2693–2696, 1997.

Crewell, S., D. Cheng, R. L. de Zafra, and C. Trimble, Millimeter wave spectroscopic measurements over the South Pole, 1. A study of stratospheric dynamics using N_2O observations, *J. Geophys. Res.*, *100*, 20,839–20,844, 1995.

Dahlberg, S. P., and K. P. Bowman, Climatology of large-scale isentropic mixing in the Arctic winter stratosphere from analyzed winds, *J. Geophys. Res.*, *99*, 20,585–20,599, 1994.

David, S. J., F. J. Murcray, A. Goldman, C. P. Rinsland, and D. G. Murcray, The effect of the Mt. Pinatubo aerosol on the HNO_3 column over Mauna Loa, Hawaii, *Geophys. Res. Lett.*, *21*, 1003–1006, 1994.

de Zafra, R. L., V. Chan, S. Crewell, C. Trimble, and J. M. Reeves, Millimeter wave spectroscopic measurements over the South Pole, 3. The behavior of stratospheric nitric acid through polar fall, winter, and spring, *J. Geophys. Res.*, *102*, 1399–1410, 1997.

Donovan, D. P., J. C. Bird, J. A. Whiteway, T. J. Duck, S. R. Pal, A. I. Carswell, J. W. Sandilands, and J. W. Kaminski, Ozone and aerosol observed by lidar in the Canadian Arctic during the winter of 1995/96, *Geophys. Res. Lett.*, *23*, 3317–3320, 1996.

Evans, W. F. J., C. T. McElroy, and I. E. Galbally, The conversion of N_2O_5 to HNO_3 at high latitudes in winter, *Geophys. Res. Lett.*, *12*, 825–828, 1985.

Fahey, D. H., S. Solomon, S. R. Kawa, M. Loewenstein, J. R. Podolske, S. E. Strahan, and K. R. Chan, A diagnostic for denitrification in the winter polar stratospheres, *Nature*, *345*, 698–702, 1990.

Fishbein, E. F., et al., Validation of UARS Microwave Limb Sounder temperature and pressure measurements, *J. Geophys. Res.*, *101*, 9983–10,016, 1996.

Froidevaux, L., et al., Validation of the UARS Microwave Limb Sounder ozone measurements, *J. Geophys. Res.*, *101*, 10,017–10,060, 1996.

Fromm, M. D., J. D. Lumpe, R. M. Bevilacqua, E. P. Shettle, J. Hornstein, S. T. Massie, and K. H. Fricke, Observations of Antarctic polar stratospheric clouds by POAM II: 1994–1996, *J. Geophys. Res.*, *102*, 23,659–23,672, 1997.

Gille, J. C., and J. M. Russell, III, The Limb Infrared Monitor of the Stratosphere: Experiment description, performance, and results, *J. Geophys. Res.*, *89*, 5125–5140, 1984.

Gille, J. C., P. L. Bailey, and C. A. Craig, Revised reference model for nitric acid, *Adv. Space Res.*, *18*, 125–138, 1996.

Girard, A., L. Gramont, N. Louisnard, S. Le Boiteux, and G. Fergant, Latitudinal variation of HNO_3, HCl, and HF vertical column density above 11.5 km, *Geophys. Res. Lett.*, *9*, 135–138, 1982.

Hanson, D., and K. Mauersberger, Laboratory studies of the nitric acid trihydrate: Implications for the south polar stratosphere, *Geophys. Res. Lett.*, *15*, 855–858, 1988.

Hofmann, D. J., and S. Solomon, Ozone destruction through heterogeneous chemistry following the eruption of El Chichòn, *J. Geophys. Res.*, *94*, 5029–5041, 1989.

Jackman, C. H., P. D. Guthrie, and J. A. Kaye, An intercomparison of nitrogen-containing species in Nimbus 7 LIMS and SAMS data, *J. Geophys. Res.*, *92*, 995–1008, 1987.

Jones, N. B., M. Koike, W. A. Matthews, and B. M. McNamara, Southern hemisphere mid-latitude seasonal cycle in total column nitric acid, *Geophys. Res. Lett.*, *21*, 593–596, 1994.

Karcher, F., M. Amodei, G. Armand, C. Besson, B. Dufour, G. Froment, and J. P. Meyer, Simultaneous measurements of HNO_3, NO_2, HCl, O_3, N_2O, CH_4, H_2O, and CO and their latitudinal variations as deduced from airborne infrared spectrometry, *Ann. Geophysicae*, *6*, 425–444, 1988.

Keim, E. R., et al., Measurements of the NO*y*-N_2O correlation in the lower stratosphere: Latitudinal and seasonal changes and model comparisons, *J. Geophys. Res.*, *102*, 13,193–13,212, 1997.

Keys, J. G., P. V. Johnston, R. D. Blatherwick, and F. J. Murcray, Evidence for heterogeneous reactions in the Antarctic autumn stratosphere, *Nature*, *361*, 49–51, 1993.

Klein, U., S. Crewell, and R. De Zafra, Correlated millimeter wave measurements of ClO, N_2O and HNO_3 from McMurdo, Antarctica, during polar spring 1994, *J. Geophys. Res.*, *101*, 20,925–20,932, 1996.

Koike, M., N. B. Jones, W. A. Matthews, P. V. Johnston, R. L. McKenzie, D. Kinnison, and J. Rodriguez, Impact of Pinatubo aerosols on the partitioning between NO_2 and HNO_3, *Geophys. Res. Lett.*, *21*, 597–600, 1994.

Kumer, J. B., et al., Comparison of correlative data with HNO_3 version 7 from the CLAES instrument deployed on the NASA Upper Atmosphere Research Satellite, *J. Geophys. Res.*, *101*, 9621–9656, 1996.

Lahoz, W. A., et al., Validation of the UARS microwave limb sounder 183 GHz H_2O measurements, *J. Geophys. Res.*, *101*, 10,129–10,149, 1996.

Lazrus, A. L., and B. W. Gandrud, Distribution of stratospheric nitric acid vapor, *J. Atmos. Sci.*, *31*, 1102–1108, 1974.

Mankin, W. G., M. T. Coffey, A. Goldman, M. R. Schoeberl, L. R. Lait, and P. A. Newman, Airborne measurements of stratospheric constituents over the Arctic in the winter of 1989, *Geophys. Res. Lett.*, *17*, 473–476, 1990.

Manney, G. L., and R. W. Zurek, Interhemispheric comparison of the development of the stratospheric polar vortex during fall: A 3-dimensional perspective for 1991–92, *Geophys. Res. Lett.*, *20*, 1275–1278, 1993.

Manney, G. L., R. W. Zurek, M. E. Gelman, A. J. Miller, and R. Nagatani, The anomalous Arctic lower stratospheric polar vortex of 1992–1993, *Geophys. Res. Lett.*, *21*, 2405–2408, 1994a.

Manney, G. L., R. W. Zurek, A. O'Neill, and R. Swinbank, On the motion of air through the stratospheric polar vortex, *J. Atmos. Sci.*, *51*, 2973–2994, 1994b.

Manney, G. L., L. Froidevaux, J. W. Waters, M. L. Santee, W. G. Read, D. A. Flower, R. F. Jarnot, and R. W. Zurek, Arctic ozone depletion observed by UARS MLS during the 1994–95 winter, *Geophys. Res. Lett.*, *23*, 85–88, 1996a.

Manney, G. L., R. Swinbank, S. T. Massie, M. E. Gelman, A. J. Miller, R. Nagatani, A. O'Neill, and R. W. Zurek, Comparison of U. K. Meteorological Office and U. S. National Meteorological Center stratospheric analyses during northern and southern winter, *J. Geophys. Res.*, *101*, 10,311–10,334, 1996b.

Mergenthaler, J. L., J. B. Kumer, A. E. Roche, and S. T. Massie, Distribution of Antarctic polar stratospheric clouds as seen by the CLAES experiment, *J. Geophys. Res.*, *102*, 19,161–19,170, 1997.

Morrey, M. W., and R. S. Harwood, Interhemispheric differences in stratospheric water vapour during late winter, in version 4 MLS measurements, *Geophys. Res. Lett.*, *25*, 147–150, 1998.

Müller, R., P. J. Crutzen, J.-U. Grooß, C. Brühl, J. M. Russell, III, and A. F. Tuck, Chlorine activation and ozone depletion in the Arctic vortex: Observations by the Halogen Occultation Experiment on the Upper Atmosphere Research Satellite, *J. Geophys. Res.*, *101*, 12,531–12,554, 1996.

Murcray, D. G., T. G. Kyle, F. H. Murcray, and W. J. Williams, Nitric acid and nitric oxide in the lower stratosphere, *Nature*, *218*, 78–79, 1968.

Murcray, D. G., D. B. Barker, J. N. Brooks, A. Goldman, and W. J. Williams, Seasonal and latitudinal variation of the stratospheric concentration of HNO_3, *Geophys. Res. Lett.*, *2*, 223–225, 1975.

Notholt, J., G. Toon, F. Stordal, S. Solberg, N. Schmidbauer, E. Becker, A. Meier, and B. Sen, Seasonal variations of atmospheric trace gases in the high Arctic at 79°N, *J. Geophys. Res.*, *102*, 12,855–12,861, 1997.

O'Neill, A., and V. D. Pope, The seasonal evolution of the extra-tropical stratosphere in the southern and northern hemispheres: Systematic changes in potential vorticity and the non-conservative effects of radiation, in *Dynamics, Transport and Photochemistry in the Middle Atmosphere of the Southern Hemisphere*, edited by A. O'Neill, pp. 33–54. Kluwer Academic Publishers, Dordrecht, The Netherlands, 1990.

Pfeilsticker, K., et al., Aircraft-borne detection of stratospheric column amounts of O_3, $ClNO_3$, HNO_3, and aerosols around the arctic vortex (79°N to 39°N) during spring 1993, 1. Observational data, *J. Geophys. Res.*, *102*, 10,801–10,814, 1997.

Poole, L. R., and M. C. Pitts, Polar stratospheric cloud climatology based on Stratospheric Aerosol Measurement II observations from 1978 to 1989, *J. Geophys. Res.*, *99*, 13,083–13,089, 1994.

Reihs, C. M., D. M. Golden, and M. A. Tolbert, Nitric acid uptake by sulfuric acid solutions under stratospheric conditions: Determination of Henry's law solubility, *J. Geophys. Res.*, *95*, 16,545–16,550, 1990.

Rinsland, C. P., R. Zander, and P. Demoulin, Ground-based infrared measurements of HNO_3 total column abundances: Long-term trend and variability, *J. Geophys. Res.*, *96*, 9379–9389, 1991.

Rinsland, C. P., et al., Heterogeneous conversion of N_2O_5 to HNO_3 in the post-Pinatubo eruption stratosphere, *J. Geophys. Res.*, *99*, 8213–8219, 1994.

Roche, A. E., et al., Observations of lower-stratospheric $ClONO_2$, HNO_3, and aerosol by the UARS CLAES experiment between January 1992 and April 1993, *J. Atmos. Sci.*, *51*, 2877–2902, 1994.

Rood, R. B., J. A. Kaye, A. R. Douglas, D. J. Allen, S. Steenrod, and E. M. Larson, Wintertime nitric acid chemistry: Implications from three-dimensional model calculations, *J. Atmos. Sci.*, *47*, 2696–2709, 1990.

Rood, R. B., A. R. Douglas, J. A. Kaye, and D. B. Considine, Characteristics of wintertime and autumn nitric acid chemistry as defined by Limb Infrared Monitor of the Stratosphere (LIMS) data, *J. Geophys. Res.*, *98*, 18,533–18,545, 1993.

Russell, III, J. M., C. B. Farmer, C. P. Rinsland, R. Zander, L. Froidevaux, G. C. Toon, B. Gao, J. Shaw, and M. Gunson, Measurements of odd nitrogen compounds in the stratosphere by the ATMOS experiment on Spacelab 3, *J. Geophys. Res.*, *93*, 1718–1736, 1988.

Santee, M. L., W. G. Read, J. W. Waters, L. Froidevaux, G. L. Manney, D. A. Flower, R. F. Jarnot, R. S. Harwood, and G. E. Peckham, Interhemispheric differences in polar stratospheric HNO_3, H_2O, ClO, and O_3, *Science*, *267*, 849–852, 1995.

Santee, M. L., et al., Chlorine deactivation in the lower stratospheric polar regions during late winter: Results from UARS, *J. Geophys. Res.*, *101*, 18,835–18,859, 1996a.

Santee, M. L., G. L. Manney, W. G. Read, L. Froidevaux, and J. W. Waters, Polar vortex conditions during the 1995–96 Arctic winter: MLS ClO and HNO_3, *Geophys. Res. Lett.*, *23*, 3207–3210, 1996b.

Santee, M. L., G. L. Manney, L. Froidevaux, R. W. Zurek, and J. W. Waters, MLS observations of ClO and HNO_3 in the 1996–97 Arctic polar vortex, *Geophys. Res. Lett.*, *24*, 2713–2716, 1997.

Santee, M. L., A. Tabazadeh, G. L. Manney, R. J. Salawitch, L. Froidevaux, W. G. Read, and J. W. Waters, UARS MLS HNO_3 observations: Implications for Antarctic polar stratospheric clouds, *J. Geophys. Res.*, *103*, 13,285–13,314, 1998.

Schoeberl, M. R., and D. L. Hartmann, The dynamics of the stratosphere polar vortex and its relation to springtime ozone depletions, *Science*, *251*, 46–52, 1991.

Schoeberl, M. R., L. R. Lait, P. A. Newman, and J. E. Rosenfield, The structure of the polar vortex, *J. Geophys. Res.*, *97*, 7859–7882, 1992.

Slusser, J., X. Liu, K. Stamnes, G. Shaw, R. Smith, R. Storvold, F. Murcray, A. Lee, and P. Good, High-latitude stratospheric NO_2 and HNO_3 over Fairbanks (65°n) 1992–1994, *J. Geophys. Res.*, *103*, 1549–1554, 1998.

Solomon, S., Progress towards a quantitative understanding of Antarctic ozone depletion, *Nature*, *347*, 347–354, 1990.

Swinbank, R., and A. O'Neill, A stratosphere-troposphere data assimilation system, *Mon. Weather Rev.*, *122*, 686–702, 1994.

Toon, G. C., C. B. Farmer, L. L. Lowes, P. W. Schaper, J.-F. Blavier, and R. H. Norton, Infrared aircraft measurements of stratospheric composition over Antarctica during September 1987, *J. Geophys. Res.*, *94*, 16,571–16,596, 1989a.

Toon, G. C., C. B. Farmer, P. W. Schaper, L. L. Lowes, and R. H. Norton, Composition measurements of the 1989 Arctic winter stratosphere by airborne infrared solar absorption spectroscopy, *J. Geophys. Res.*, *97*, 7939–7961, 1992.

Toon, O. B., R. P. Turco, J. Jordan, J. Goodman, and G. Ferry, Physical processes in polar stratospheric ice clouds, *J. Geophys. Res.*, *94*, 11,359–11,380, 1989b.

Tuck, A. F., D. W. Fahey, M. Loewenstein, J. R. Podolske, K. K. Kelly, S. J. Hovde, D. M. Murphy, and J. W. Elkins, Spread of denitrification from 1987 Antarctic and 1988–1989 Arctic stratospheric vortices, *J. Geophys. Res.*, *99*, 20,573–20,583, 1994.

Turco, R. P., O. B. Toon, and P. Hamill, Heterogeneous physicochemistry of the polar ozone hole, *J. Geophys. Res.*, *94*, 16,493–16,510, 1989.

Van Allen, R., X. Liu, and F. J. Murcray, Seasonal variation of atmospheric nitric acid over the south pole in 1992, *Geophys. Res. Lett.*, *22*, 49–52, 1995.

Waters, J. W., Microwave limb sounding, in *Atmospheric Remote Sensing by Microwave Radiometry*, edited by M. A. Janssen, chap. 8, pp. 383–496. John Wiley & Sons, New York, 1993.

Waters, J. W., et al., The UARS and EOS Microwave Limb Sounder (MLS) experiments, *J. Atmos. Sci.*, in press, 1998.

Waters, J. W., L. Froidevaux, W. G. Read, G. L. Manney, L. S. Elson, D. A. Flower, R. F. Jarnot, and R. S. Harwood, Stratospheric ClO and ozone from the Microwave Limb Sounder on the Upper Atmosphere Research Satellite, *Nature*, *362*, 597–602, 1993.

Waugh, D. W., and W. J. Randel, Climatology of Arctic and Antarctic polar vortices using elliptical diagnostics, *J. Atmos. Sci.*, in press, 1998.

Webster, C. R., R. D. May, M. Allen, L. Jaegle, and M. P. McCormick, Balloon profiles of stratospheric NO_2 and HNO_3 for testing the heterogeneous hydrolysis of N_2O_5 on sulfate aerosols, *Geophys. Res. Lett.*, *21*, 53–56, 1994.

Williams, W. J., J. J. Kosters, and D. G. Murcray, Nitric acid column densities over Antarctica, *J. Geophys. Res.*, *87*, 8976–8980, 1982.

Zurek, R. W., G. L. Manney, A. J. Miller, M. E. Gelman, and R. M. Nagatani, Interannual variability of the north polar vortex in the lower stratosphere during the UARS mission, *Geophys. Res. Lett.*, *23*, 289–292, 1996.

L. Froidevaux, G. L. Manney, W. G. Read, M. L. Santee (corresponding author), and J. W. Waters, Jet Propulsion Laboratory, Mail Stop 183–701, 4800 Oak Grove Drive, Pasadena, CA 91109. (e-mail: mls@mls.jpl.nasa.gov)

Received _____

Submitted to JGR-Atmospheres, August 1998

This manuscript was prepared with AGU's LaTeX macros v4, with the extension package 'AGU++' by P. W. Daly, version 1.5d from 1997/04/28.

Figure Captions

Plate 1. Maps of MLS HNO_3 (parts per billion by volume, ppbv) for selected days during each of the five south-looking yaw periods that occur each year, for the years 1991–92 to 1997–98 (see text and Table 1). Maps are missing for days on which no MLS data are available. The data have been interpolated onto the 465-K potential temperature surface using UKMO temperatures. The maps are polar orthographic projections extending to the equator, with the Greenwich meridian at the top and with dashed black circles at 30°S and 60°S; blank spaces represent data gaps or bad data points. Superimposed in white are two contours of UKMO potential vorticity (PV): -0.25×10^{-4} K m^2 kg^{-1} s^{-1} (to represent the approximate edge of the winter polar vortex at this level) and -0.30×10^{-4} K m^2 kg^{-1} s^{-1} (a second contour to indicate the steepness of the PV gradient and thus the strength of the vortex). Superimposed in black are two contours of UKMO temperature: 195 K (the approximate existence threshold for type I polar stratospheric clouds (PSCs) and 188 K (the ice frost point).

Plate 2. As in Plate 1, for selected days during each of the five north-looking yaw periods in the years 1991–92 to 1996–97 (see text and Table 2), with the Greenwich meridian at the bottom and positive PV contour values.

Plate 3. Southern (left) and northern (right) hemisphere climatologies at 465 K derived by averaging together the individual days for each yaw period shown in Plates 1 or 2. Thus each climatology is based on a single day from at least 4 and at most 6 years of data. Also overlaid, as in Plates 1 and 2, are the averaged temperature and PV fields from the UKMO analyses.

Plate 4. Differences (in ppbv) from the mid-June climatology of Plate 3 for each of the mid-June days represented in Plate 1 (left) and from the mid-January climatology for each of the mid-January days (right). The -0.25×10^{-4} K m^2 kg^{-1} s^{-1} value of the averaged UKMO PV field (as in Plate 3) is shown as a solid white contour, whereas the -0.25×10^{-4} K m^2 kg^{-1} s^{-1} PV value on each individual day (as in Plate 1) is shown as a dotted white contour. Similarly, the 195 K value of the averaged UKMO temperature field is shown as a solid black contour, whereas the 195 K temperature value on each individual day is shown as a dotted black contour.

Plate 5. MLS HNO_3 at 465 K as a function of latitude for each of the individual days in Plates 1 and 2, arranged with the 5 south-looking yaw periods plotted on the left and the 5 north-looking yaw periods plotted on the right. The data for each day have been binned into 5° latitude bands and averaged. Different years are represented by different colors as indicated in the legend.

Plate 6. Time series of daily zonal-mean MLS HNO_3 at 465 K as a function of latitude for six annual cycles in both the southern (left side) and northern (right side) hemispheres, starting in early winter each year. The partial year 1997–98, which appears in the maps in Plate 1 but which includes data only from April through June 1997, is not shown. Blank spaces in the plots correspond to periods when data are missing or MLS was pointing in the opposite hemisphere.

Plate 7. Southern (top) and northern (bottom) hemisphere daily zonal-mean climatology of MLS HNO_3 at 465 K as a function of latitude, obtained by averaging together for the respective hemispheres the results for the six individual years shown in Plate 6 plus the partial year 1997–98.

Plate 8. Time series of MLS HNO_3 at 465 K binned into 5° latitude bands and averaged, for the southern (left) and northern (right) hemispheres. Different years are represented by different colors as indicated in the legend. Daily averages calculated from the southern hemisphere data points in every year are overlaid on the northern hemisphere plot as a black line (shifted by six months so that comparable seasons are aligned). To facilitate comparison, the daily averages calculated from the northern hemisphere data points are also overlaid on the northern hemisphere plot as a grey line. Dotted vertical lines demark calendar months.

Plate 9. Time series of MLS HNO_3 at 465 K averaged over vortex "inner core" (left, defined by $PV > 0.48 \times 10^{-4}$ K m^2 kg^{-1} s^{-1}) and "collar" (right, defined by 0.25×10^{-4} K m^2 kg^{-1} s^{-1} < $PV < 0.40 \times 10^{-4}$ K m^2 kg^{-1} s^{-1}) regions. Different years are represented by different colors as in Plate 8. Average (thick black line) and minimum (thin black line) UKMO temperatures in these regions are also shown. Horizontal grey lines denote temperatures of 185, 188, 190, and 195 K. Dotted vertical lines demark calendar months. Note that the horizontal axis has been expanded since only the three yaw periods during which the highest PV values exist are depicted.

Tables

Table 1. Days Selected From Each of the 5 South-looking Yaw Periods in Each Year

year	early-April	mid-June	late-August	early-November	mid-January
1991–92	–	–	–	4 Nov	20 Jan
1992–93	1 Apr	15 Jun	26 Aug	4 Nov	20 Jan
1993–94	1 Apr	15 Jun	26 Aug	4 Nov	20 Jan
1994–95	1 Apr	15 Jun	26 Aug	5 Nov	–
1995–96	–	14 Jun	26 Aug	4 Nov	19 Jan
1996–97	2 Apr	15 Jun	26 Aug	4 Nov	–
1997–98	1 Apr	14 Jun	–	–	–

Table 2. Days Selected From Each of the 5 North-looking Yaw Periods in Each Year

year	early-October	mid-December	late-February	late-April	mid-July
1991–92	–	20 Dec	26 Feb	2 May	18 Jul
1992–93	1 Oct	20 Dec	26 Feb	30 Apr	18 Jul
1993–94	1 Oct	20 Dec	26 Feb	29 Apr	18 Jul
1994–95	1 Oct	21 Dec	28 Feb	–	–
1995–96	5 Oct	20 Dec	26 Feb	30 Apr	18 Jul
1996–97	2 Oct	18 Dec	26 Feb	30 Apr	–

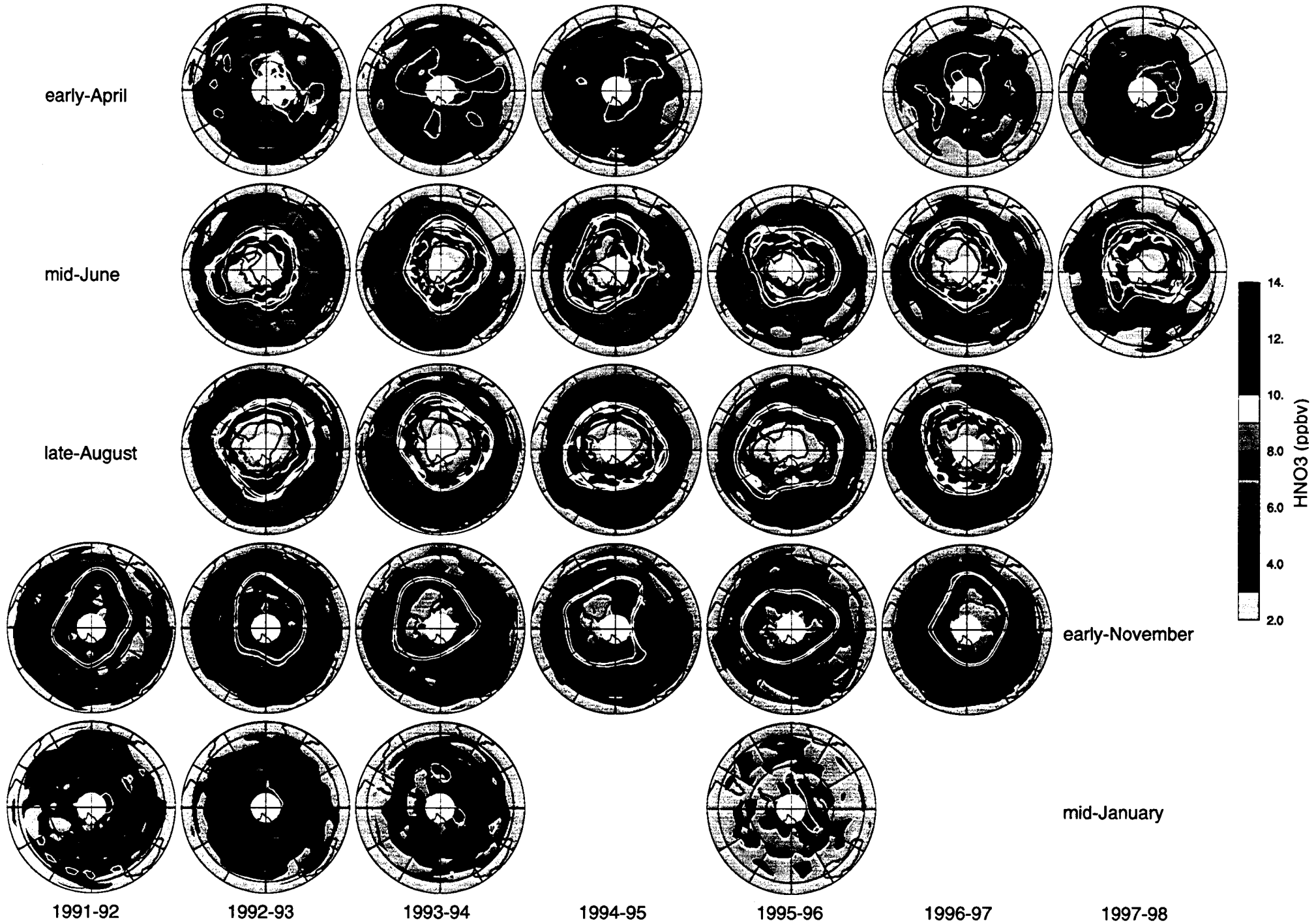
early-April
mid-June
late-August
early-November
mid-January
14.
12.
10.
8.0
6.0
4.0
2.0
HNO3 (ppbv)
1991-92
1992-93
1993-94
1994-95
1995-96
1996-97
1997-98

Plate 1

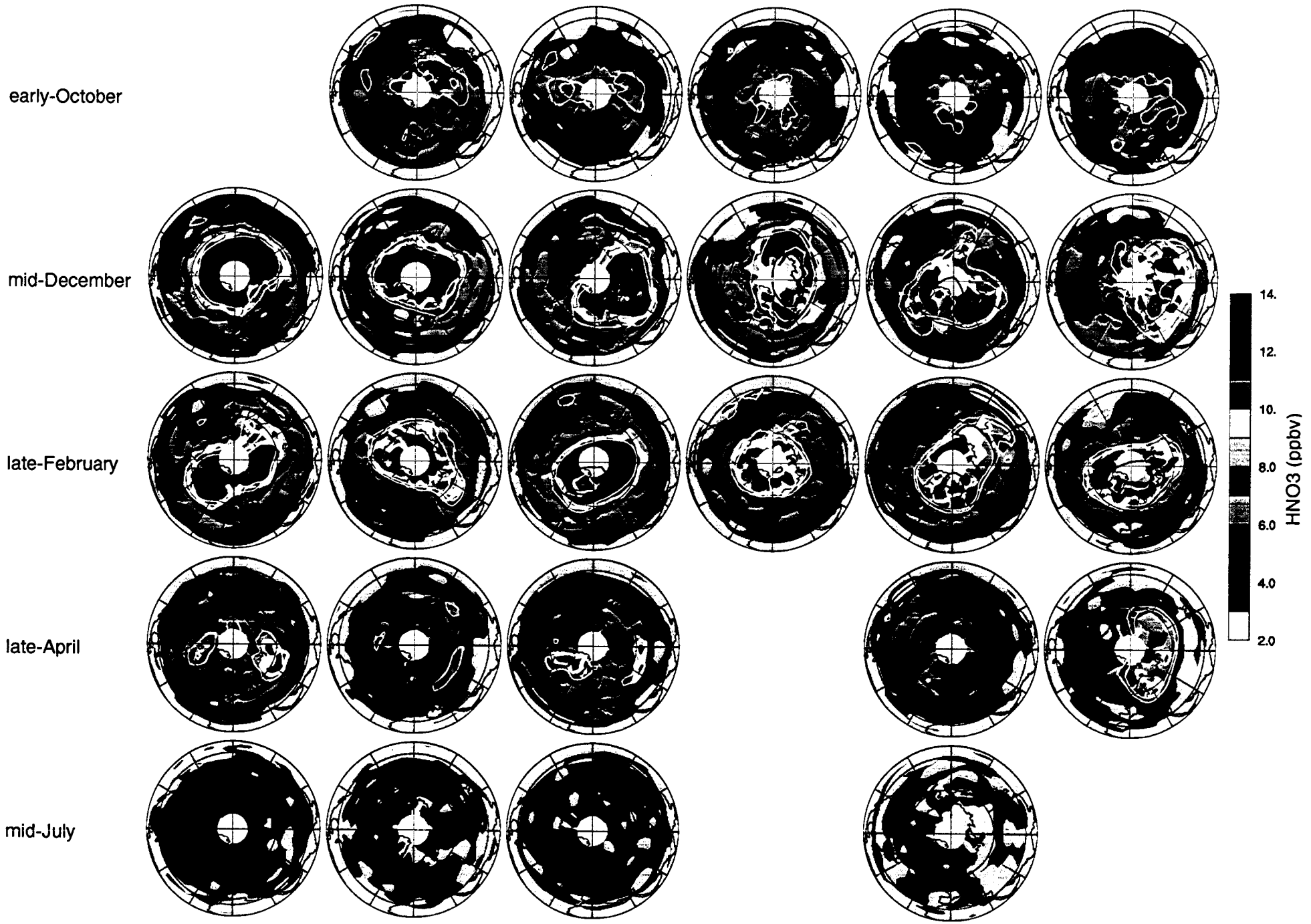
early-October
mid-December
late-February
late-April
mid-July
1991-92
1992-93
1993-94
1994-95
1995-96
1996-97
14.
12.
10.
8.0
6.0
4.0
2.0
HNO3 (ppbv)

Plate 2

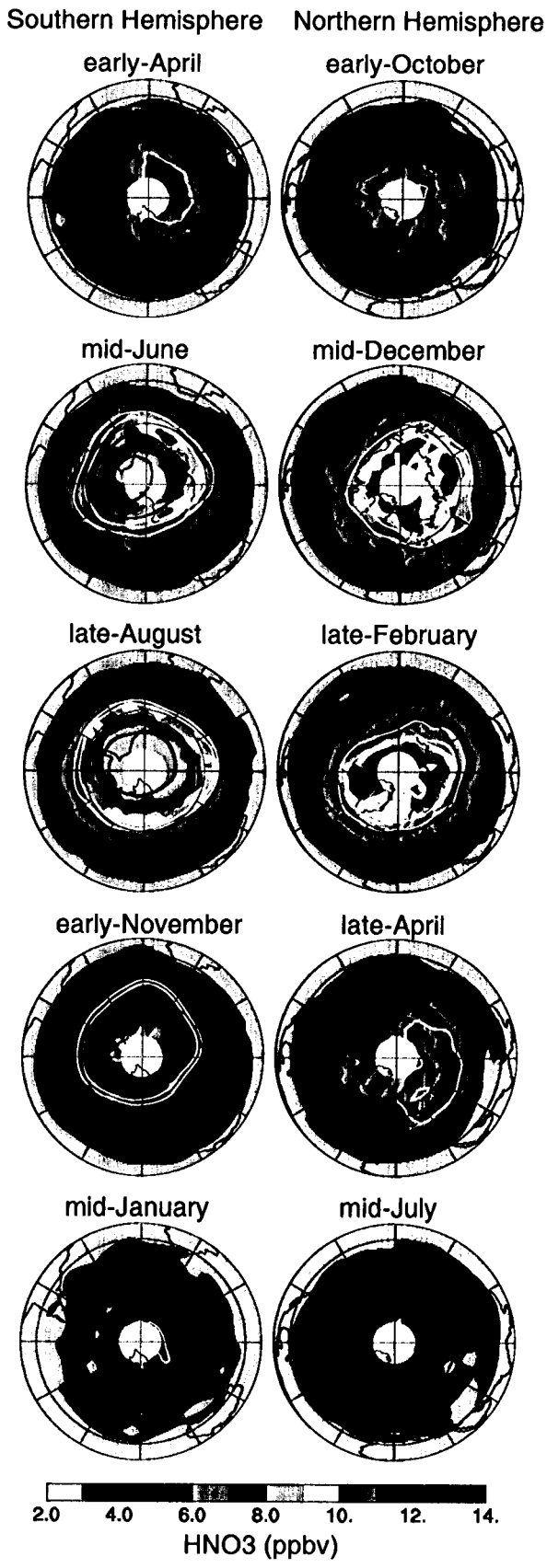
Southern Hemisphere
Northern Hemisphere
early-April
early-October
mid-June
mid-December
late-August
late-February
early-November
late-April
mid-January
mid-July
2.0
4.0
6.0
8.0
10.
12.
14.
HNO3 (ppbv)

[Plate 3]

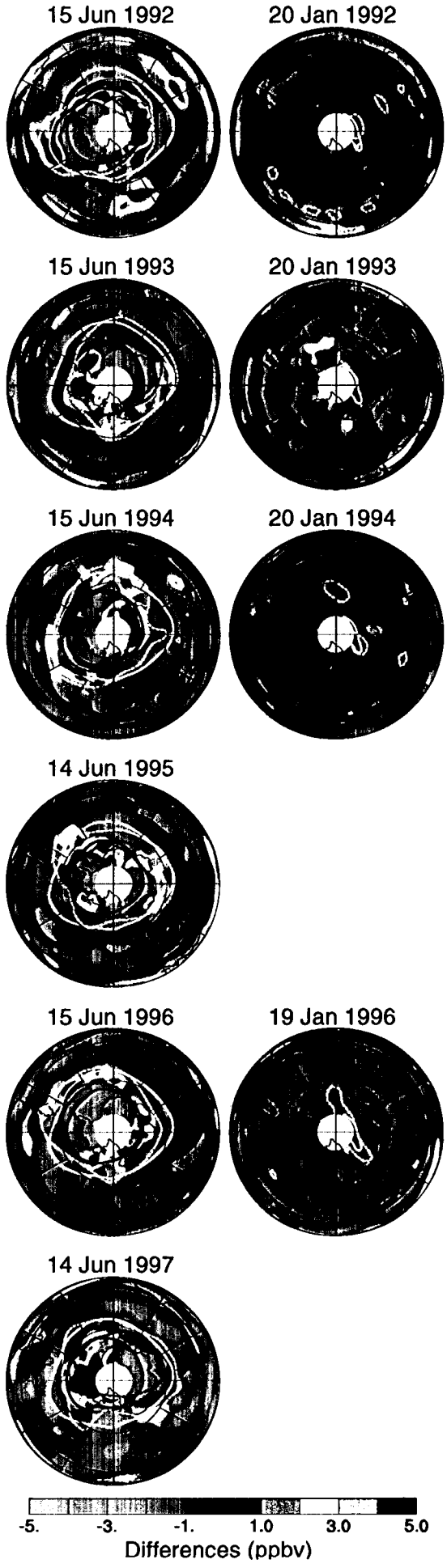
15 Jun 1992
20 Jan 1992
15 Jun 1993
20 Jan 1993
15 Jun 1994
20 Jan 1994
14 Jun 1995
15 Jun 1996
19 Jan 1996
14 Jun 1997
-5.
-3.
-1.
1.0
3.0
5.0
Differences (ppbv)

Plate 11

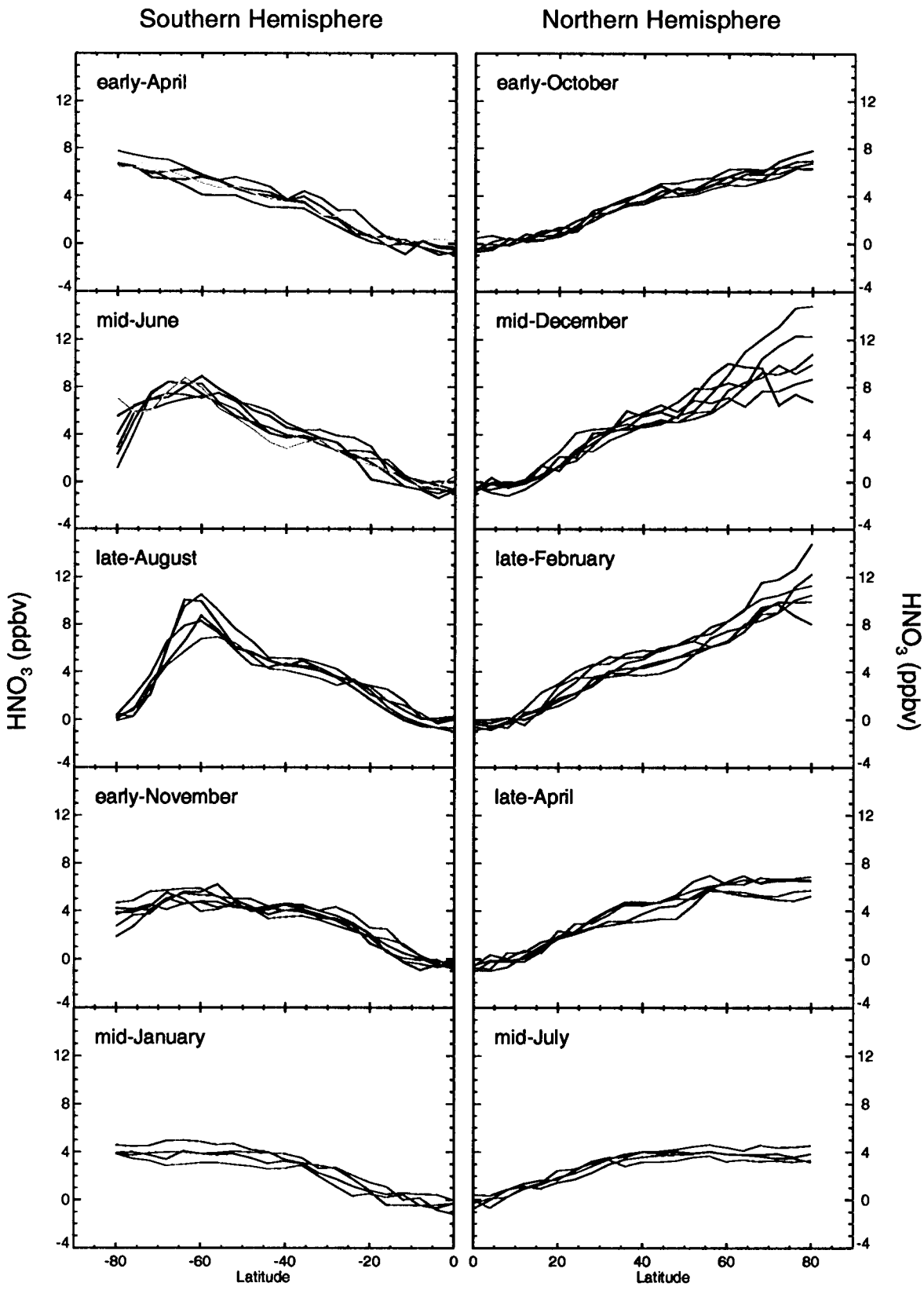
Southern Hemisphere
Northern Hemisphere
early-April
early-October
mid-June
mid-December
late-August
late-February
early-November
late-April
mid-January
mid-July
HNO3 (ppbv)
HNO3 (ppbv)
Latitude
Latitude
1991-92
1992-93
1993-94
1994-95
1995-96
1996-97
1997-98

Plate 5

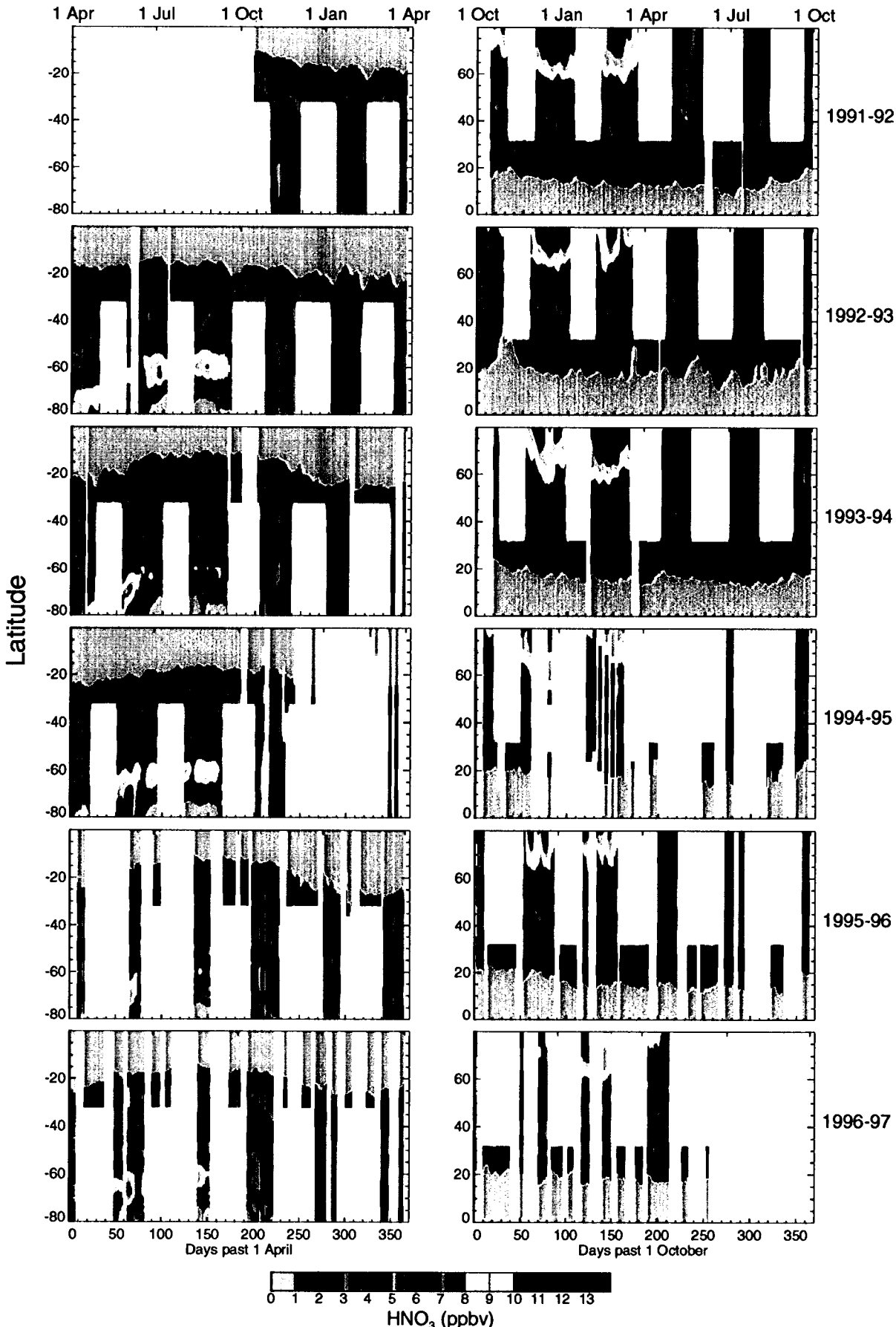
1 Apr
1 Jul
1 Oct
1 Jan
1 Apr
1 Oct
1 Jan
1 Apr
1 Jul
1 Oct
Latitude
1991-92
1992-93
1993-94
1994-95
1995-96
1996-97
Days past 1 April
Days past 1 October
0 1 2 3 4 5 6 7 8 9 10 11 12 13
HNO3 (ppbv)

Plate 6

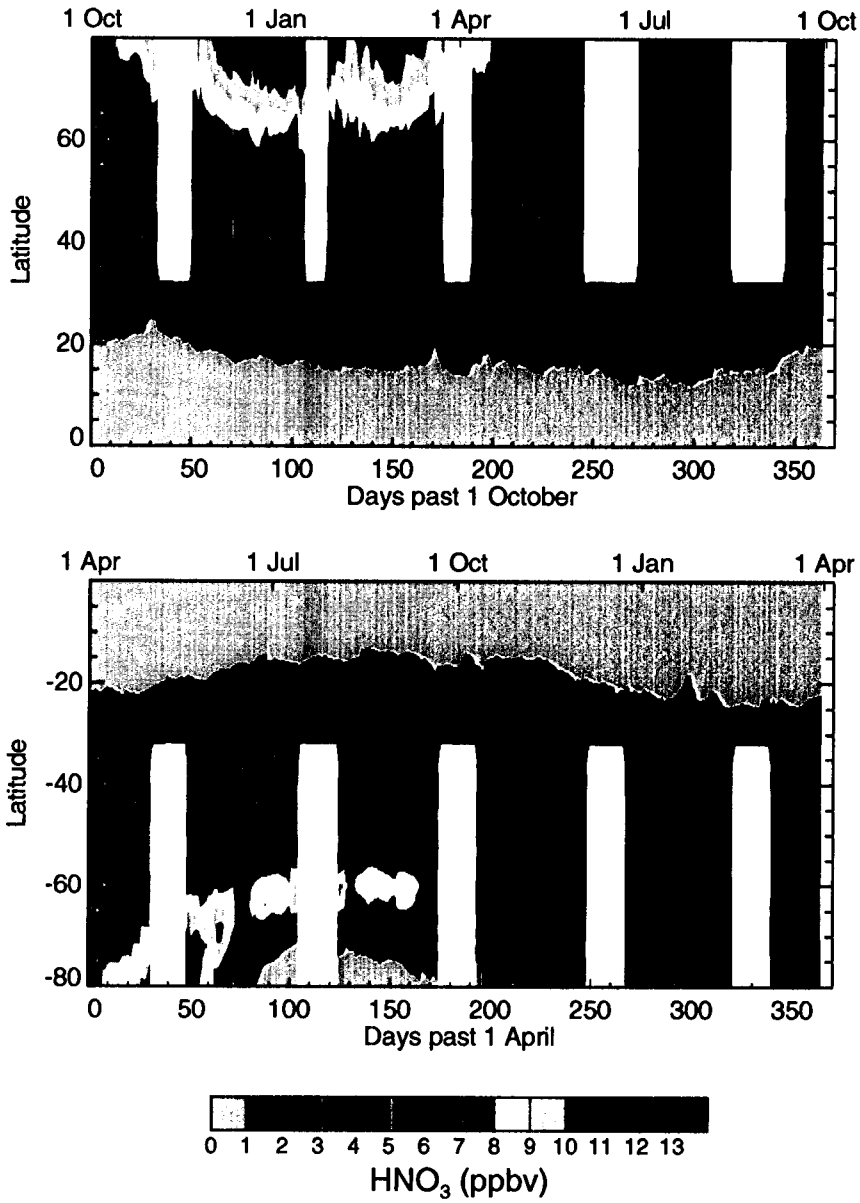
1 Oct
1 Jan
1 Apr
1 Jul
1 Oct
Latitude
60
40
20
0
0 50 100 150 200 250 300 350
Days past 1 October
1 Apr
1 Jul
1 Oct
1 Jan
1 Apr
Latitude
-20
-40
-60
-80
0 50 100 150 200 250 300 350
Days past 1 April
0 1 2 3 4 5 6 7 8 9 10 11 12 13
HNO3 (ppbv)

Plate 7

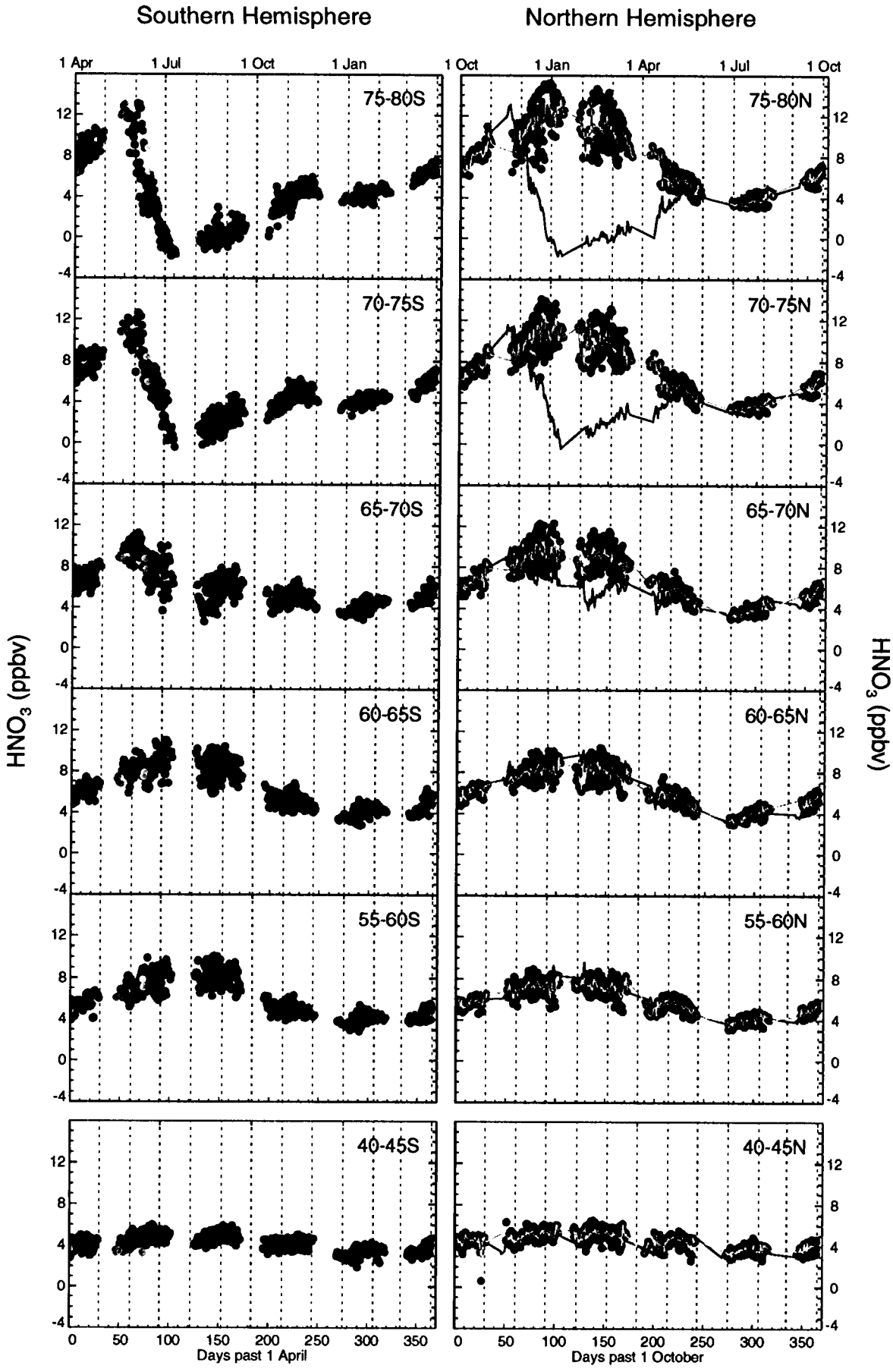
Southern Hemisphere
Northern Hemisphere
1 Apr
1 Jul
1 Oct
1 Jan
1 Oct
1 Jan
1 Apr
1 Jul
1 Oct
75-80S
75-80N
70-75S
70-75N
65-70S
65-70N
60-65S
60-65N
55-60S
55-60N
40-45S
40-45N
HNO3 (ppbv)
HNO3 (ppbv)
12
8
4
0
-4
0
50
100
150
200
250
300
350
Days past 1 April
Days past 1 October
1991-92
1992-93
1993-94
1994-95
1995-96
1996-97
1997-98

Plate 8

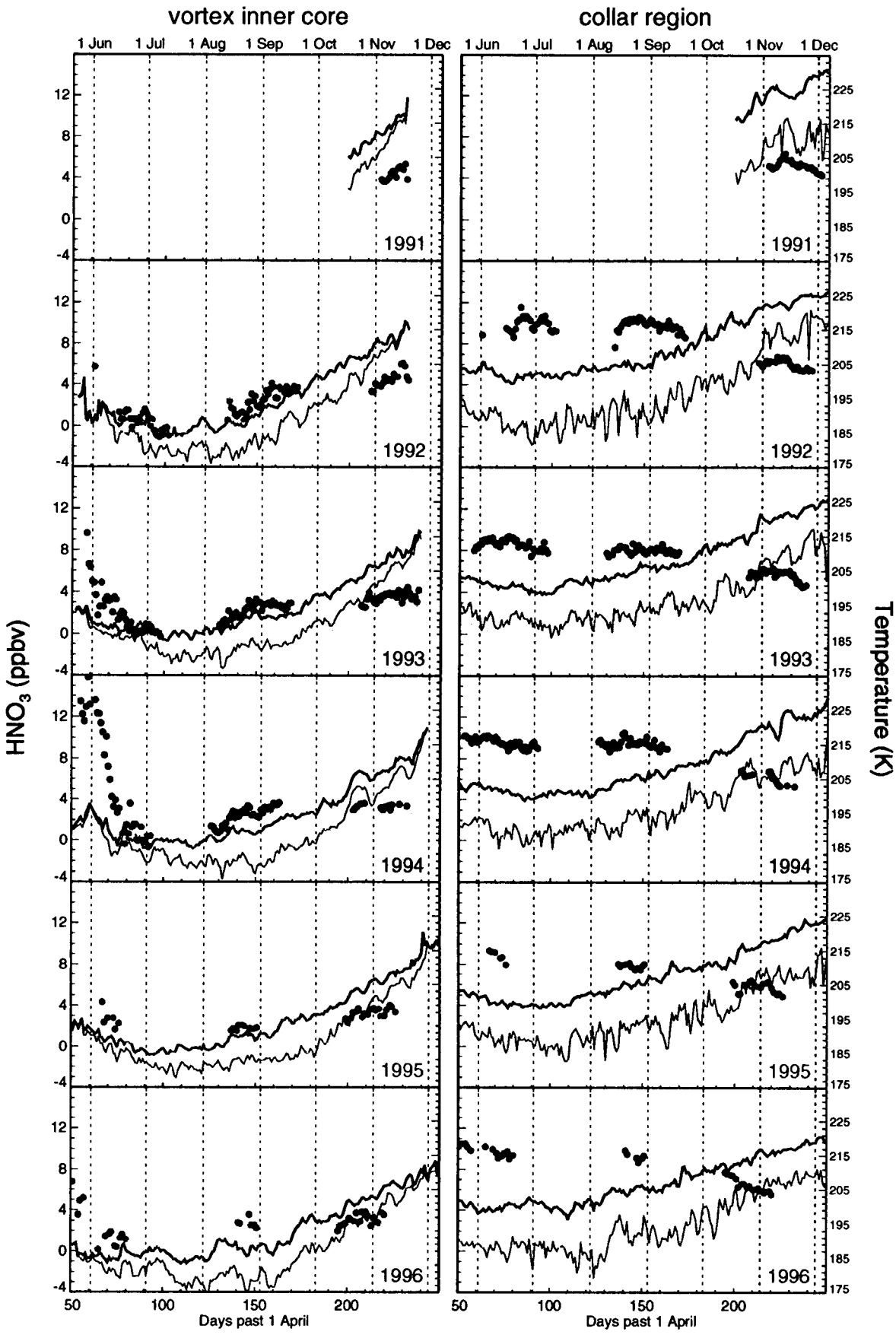
vortex inner core
collar region
1 Jun
1 Jul
1 Aug
1 Sep
1 Oct
1 Nov
1 Dec
1991
1992
1993
1994
1995
1996
HNO3 (ppbv)
Temperature (K)
Days past 1 April
50
100
150
200

Plate 9